CANCER

Protein kinase C delta regulates mononuclear phagocytes and hinders response to immunotherapy in cancer

Mehdi Chaib[1], Jeremiah R. Holt[2], Emilie L. Fisher[3], Laura M. Sipe[2]†, Margaret S. Bohm[4], Sydney C. Joseph[2], Boston W. Simmons[2], Samson Eugin Simon[2], Johnathan R. Yarbro[2], Ubaid Tanveer[2], Jessica L. Halle[5], James A. Carson[5], T.J. Hollingsworth[4,6,7], QingQing Wei[8], Jeffrey C. Rathmell[3], Paul G. Thomas[4,9], D. Neil Hayes[2,10], Liza Makowski[1,2,4,10]*

Mononuclear phagocytes (MPs) play a crucial role in tissue homeostasis; however, MPs also contribute to tumor progression and resistance to immune checkpoint blockade (ICB). Targeting MPs could be an effective strategy to enhance ICB efficacy. We report that protein kinase C delta (PKCδ), a serine/threonine kinase, is abundantly expressed by MPs in human and mouse tumors. PKCδ$^{−/−}$ mice displayed reduced tumor progression compared to wild types, with increased response to anti–PD-1. Tumors from PKCδ$^{−/−}$ mice demonstrated T$_H$1-skewed immune response including increased antigen presentation and T cell activation. Depletion of MPs in vivo altered tumor growth in control but not PKCδ$^{−/−}$ mice. Coinjection of PKCδ$^{−/−}$ M2-like macrophages with cancer cells into wild-type mice markedly delayed tumor growth and significantly increased intratumoral T cell activation compared to PKCδ$^{+/+}$ controls. PKCδ deficiency reprogrammed MPs by activating type I and type II interferon signaling. Thus, PKCδ might be targeted to reprogram MPs to augment ICB efficacy.

INTRODUCTION

Tumors develop in the context of a highly complex microenvironment that can greatly influence disease progression and response to therapy (1). Immune cells are now widely recognized as a crucial component of the tumor microenvironment (TME) and are prognostic for clinical outcome in patients with cancer (2). Much of the field's focus has been on approaches that reinvigorate adaptive immunity such as the use of immune checkpoint blockade (ICB) showing unprecedented durable responses (3). Unfortunately, most patients do not respond to ICB for reasons that are still unclear (4, 5). One of the most important factors that contribute to immunotherapy resistance is the immunosuppressive nature of the TME, which is largely shaped by innate immune cells, mainly myeloid cells (6). This emphasizes the need to understand the signals that regulate myeloid cells in the TME (7).

Mononuclear phagocytes (MPs) comprising monocytes, macrophages, and dendritic cells (DCs) are a heterogenous innate immune cell population that plays a crucial role in host defense and tissue homeostasis (8). However, MPs contribute to all phases of tumorigenesis including orchestrating inflammatory events during de novo carcinogenesis, contribution to the progression of established tumors, and promotion of resistance to ICB (9, 10). Because of their highly plastic nature, MPs often play opposing roles where they orchestrate antitumor responses on one hand and promote immune suppression on the other (11). Therefore, understanding the signals that regulate MP functional states may yield powerful targets to harness the antitumor potential of innate immunity to improve cancer immunotherapy response.

Monocytes are composed of two main subsets in mice and humans, classical and nonclassical monocytes, and these cells are found predominantly in the circulation, bone marrow, and spleen (12). Both monocyte subsets have been reported to have pro- and antitumor properties (13–15). Immature myeloid cells (iMCs), also defined as monocytic myeloid-derived suppressor cells (M-MDSCs) are another subset of the monocytic lineage and are highly immunosuppressive in cancer (16, 17). Monocytes and M-MDSCs express high levels of Ly6C in mice. Both cell types also play a role in tumor progression by differentiating into monocyte-derived macrophages or monocyte-derived DCs in the TME (11, 18). Tumor-associated macrophages represent the major tumor-infiltrating immune cell type in most solid tumors and are assumed to be tumor promoting (19). DCs, on the other hand, are generally considered to be favorable for the antitumor response because of their remarkable antigen-presenting capacity (20–23). However, DCs also have regulatory functions that limit antitumor immunity (24). Consequently, identifying targets that can reprogram MPs in cancer are needed (7).

[1]Department of Pharmaceutical Sciences, College of Pharmacy, The University of Tennessee Health Science Center, Memphis, TN 38163, USA. [2]Department of Medicine, Division of Hematology and Oncology, College of Medicine, The University of Tennessee Health Science Center, Memphis, TN 38163, USA. [3]Vanderbilt Center for Immunobiology and Department of Pathology, Microbiology, and Immunology, Vanderbilt University Medical Center, Nashville, TN 37235, USA. [4]Department of Microbiology, Immunology, and Biochemistry, College of Medicine, The University of Tennessee Health Science Center, Memphis, TN 38163, USA. [5]Department of Physical Therapy, College of Health Professions, The University of Tennessee Health Science Center, Memphis, TN 38163, USA. [6]Department of Ophthalmology, Hamilton Eye Institute, College of Medicine, The University of Tennessee Health Science Center, Memphis, TN 38163, USA. [7]Department of Anatomy and Neurobiology, College of Medicine, The University of Tennessee Health Science Center, Memphis, TN 38163, USA. [8]Department of Cellular Biology and Anatomy, Augusta University, Augusta, GA 30912, USA. [9]Department of Immunology, St. Jude Children's Research Hospital, Memphis, TN 38105, USA. [10]UTHSC Center for Cancer Research, College of Medicine, The University of Tennessee Health Science Center, Memphis, TN 38163, USA.
*Corresponding author. Email: liza.makowski@uthsc.edu
†Present address: Department of Biological Sciences, College of Arts and Sciences, The University of Mary Washington, Fredericksburg VA 22401, USA.

Protein kinase C delta (PKCδ), a serine/threonine kinase, is involved in several cellular processes including differentiation, apoptosis, cell survival, and proliferation (25, 26). Autosomal recessive PKCδ deficiency in humans or genetic deletion of PKCδ in mice resulted in severe systemic autoimmunity (26–28). In myeloid cells, loss of PKCδ resulted in impaired extracellular trap formation in neutrophils (29) and decreased macrophage phagosomal clearance of microbes (30, 31). Whether PKCδ inhibits or promotes cancer cell growth is not clear from the literature (32). However, the role of PKCδ in antitumor immunity is largely unknown.

In this study, $Prkcd^{-/-}$ mice displayed delayed tumor growth compared to wild-type ($Prkcd^{+/+}$) mice using breast, lung, and melanoma cancer models. Delay of tumor growth was more significant in E0771 (breast) and Lewis cell carcinoma (LLC) (lung) models, which correlated with higher content of MPs in these tumors. The effects of PKCδ deficiency on tumor growth were associated with increased antigen presentation and intratumoral $CD8^+$ T cells, which expressed higher levels of activation markers protein death receptor 1 (PD-1), interferon-γ (IFN-γ) and tumor necrosis factor−α (TNFα). Overall, PKCδ deficiency induced a T helper 1–skewed immune response in the tumors. We also found PKCδ to be abundantly expressed by MPs across several human tumors using single-cell RNA sequencing (scRNA-seq) analysis of several publicly available databases. The depletion of MPs or MP tumor cell co-injection experiments revealed that the effects of PKCδ deficiency on tumor growth and immune suppression were dependent on MPs. Mechanistically, intrinsic loss of PKCδ in MPs activated type I and II IFN signaling and enhanced their antigen-presenting and cross-presenting capability. Last, anti−PD-1 immunotherapy was more effective in PKCδ-deficient compared to wild-type tumor-bearing mice as evidenced by a marked delay in tumor growth and a significantly longer overall survival. In summary, PKCδ represents an attractive heretofore unappreciated target to reprogram MPs and enhance ICB efficacy in cancer.

RESULTS
PKCδ promotes tumor growth and immune suppression in mice
To explore the role of PKCδ in tumorigenesis, we implanted breast (E0771), lung (LLC), and melanoma (B16F10) syngeneic murine cancer cell lines into $Prkcd^{+/+}$ and $Prkcd^{-/-}$ mice. Compared to $Prkcd^{+/+}$ mice, $Prkcd^{-/-}$ mice exhibited a significant delay in tumor growth in E0771 and LLC models (Fig. 1, A and B), but this effect was not significant in the B16F10 model (Fig. 1C). When we analyzed the intratumoral immune cell content of these tumors using flow cytometry, we found that E0771 and LLC tumors were abundantly infiltrated by MPs (27.85 and 35.79% of all viable cells, respectively), but not B16F10 tumors (1.59%) (Fig. 1D) in C57BL/6J mice, which was consistent with previously published findings (16, 33). The decreased effect in the B16F10 model harboring fewer MPs suggests that PKCδ may primarily regulate MPs in cancer.

We next examined the effect of PKCδ deficiency on gene regulation by bulk RNA-seq and analysis of differentially expressed genes (DEGs) in E0771 tumors. There were 473 significantly up-regulated and 240 significantly down-regulated genes in $Prkcd^{-/-}$ versus $Prkcd^{+/+}$ tumors (fig. S1A). Gene Ontology (GO) analysis

of genes up-regulated in $Prkcd^{-/-}$ revealed enhanced immunostimulatory responses (such as T cell activation, IFN-γ signaling, and antigen presentation) (Fig. 1E). In addition, genes involved in antigen presentation, innate immunity, and T cell activation were elevated in $Prkcd^{-/-}$ tumors compared to $Prkcd^{+/+}$ tumors (Fig. 1F). Similarly, gene set enrichment analysis (GSEA) revealed significant enrichment for multiple immune-related GO pathways in $Prkcd^{-/-}$ tumors including T cell activation, antigen processing and presentation, innate immune response, and inflammatory response (fig. S1, B to E).

Flow cytometry analysis revealed enhanced expression of major histocompatibility complex class II (MHCII) in macrophages and monocytes/iMCs ($Ly6C^{hi}$ cells) from tumors (Fig. 1, G and H) and spleens (Fig. 1, G and I) of $Prkcd^{-/-}$ compared to $Prkcd^{+/+}$ E0771 tumor-bearing mice, which is suggestive of enhanced maturation and antigen-presenting capacity of these cells. Furthermore, cell frequencies and absolute cell numbers of macrophages, Ly6C-high cells, as well as both subsets of DCs (cDC1 and cDC2) were increased in tumors from $Prkcd^{-/-}$ mice (fig. S2, A and B). We also observed a substantial increase in T cell content (total $CD3^+$ T cells and $CD4^+$ and $CD8^+$ T cells) in E0771 $Prkcd^{-/-}$ tumors by absolute quantity and frequency (Fig. 1, J and K) compared to $Prkcd^{+/+}$ tumors. There was a significant increase in $CD8^+$ T cell activation ($IFN-γ^+ TNFα^+$) in E0771 $Prkcd^{-/-}$ tumors (Fig. 1L). In $Prkcd^{-/-}$ LLC tumors, $CD8^+$ T cell content (Fig. 1M) and PD-$1^+ CD8^+$ T cells (Fig. 1N) were significantly elevated compared to $Prkcd^{+/+}$ tumors. Cumulatively, these results demonstrate that PKCδ deficiency restricts the growth of tumors that are highly infiltrated by MPs, which suggested that this restraint may be associated with changes in infiltrating MPs that may affect T cell responses.
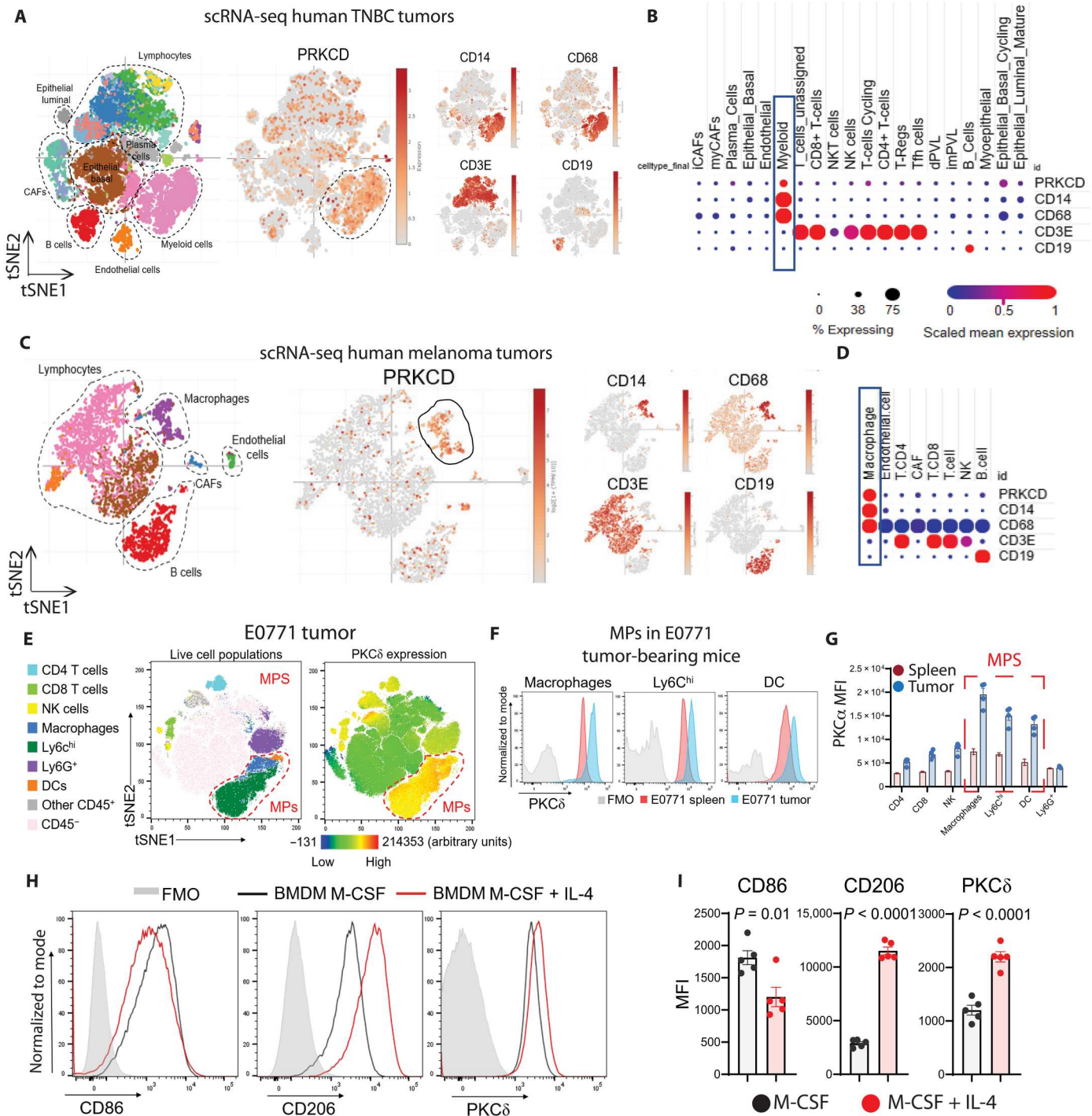
PKCδ is abundantly expressed by MPs
Because an immune response was required for tumor regression in $Prkcd^{-/-}$ mice, we asked which cells express high levels of PKCδ not only in tumors but also in organs at steady state. First, we investigated PKCδ expression at a cellular level in several human tumors using scRNA-seq analysis of publicly available datasets. We found that a substantial fraction of MPs abundantly expressed PRKCD (PKCδ gene) relative to other immune-infiltrating cells in human triple-negative breast cancer (TNBC) (Fig. 2, A and B) (34), melanoma (Fig. 2, C and D) (35), renal cell carcinoma (36), colon cancer (37), and glioblastoma (38) tumors (fig. S2, C to E, respectively). PKCδ was also abundantly expressed by MPs at steady state in human peripheral blood mononuclear cells (PBMCs; Broad/Boston and Mt. Sinai/NYC) (fig. S2F) and mouse $CD45^+$ splenocytes (ImmGen labs; fig. S2G). Using publicly available human scRNA-seq datasets, we found that PKCδ is the most abundant PKC isoform in myeloid cells pointing to an important but unappreciated role of this isoform in the regulation of myeloid cells (fig. S3).

Next, we checked PKCδ protein expression in the spleen and tumor cell populations from E0771 tumor-bearing mice using flow cytometry. We found that PKCδ was predominantly expressed by MPs in E0771 tumors (Fig. 2E) and LLC tumors (fig. S2H). In addition, MPs from E0771 tumor-bearing mice had significantly higher expression of PKCδ in the tumors compared to the spleen (Fig. 2, F and G). Notably, myeloid cells from tumors are more immunosuppressive than their counterparts in the spleens (39). PKCδ
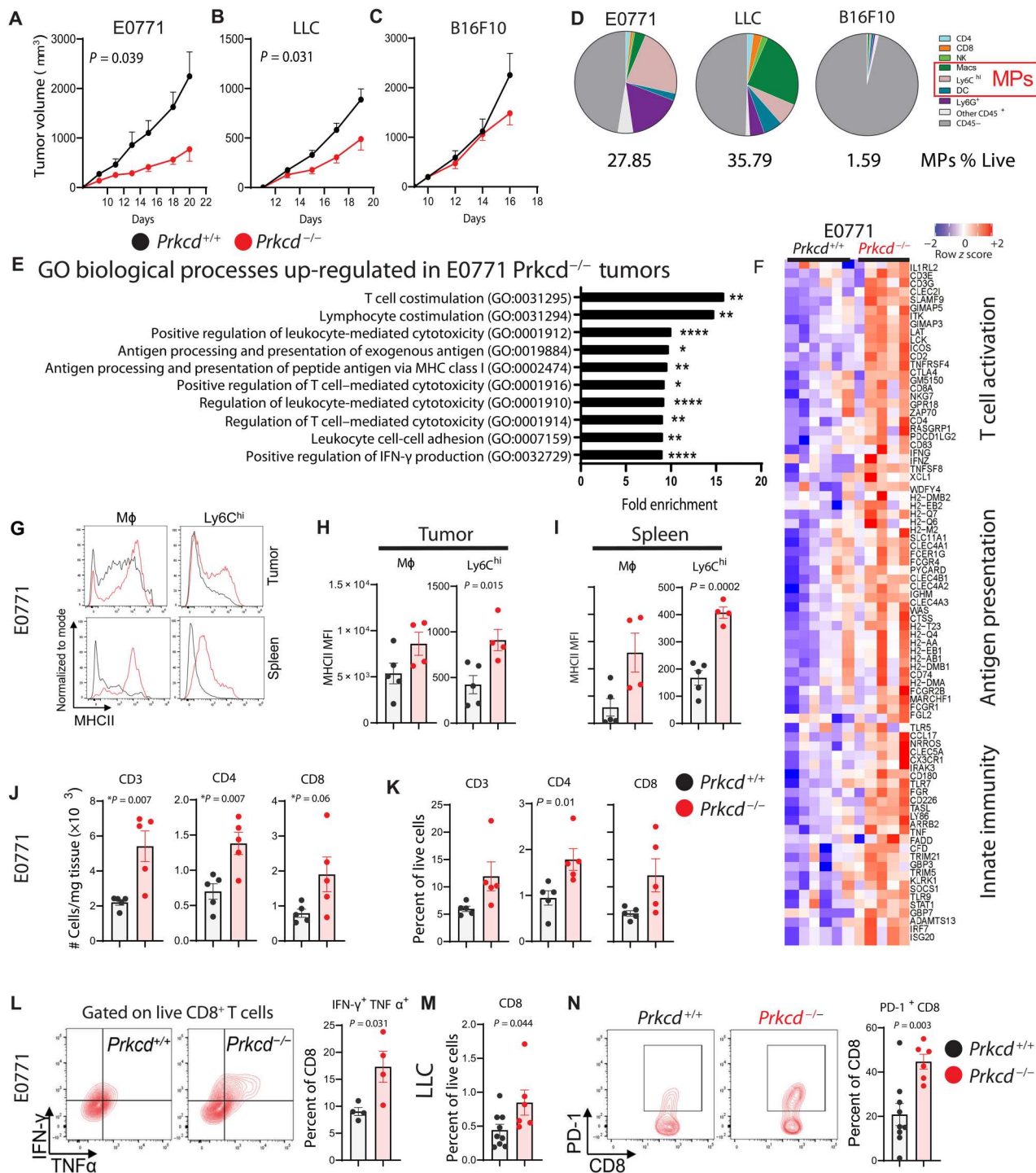
Fig. 1. PKCδ promotes tumor growth and immune suppression. (**A** to **C**) Tumor volumes in *Prkcd*^{+/+} and *Prkcd*^{−/−} mice orthotopically injected with (A) E0771 breast cancer cells (*N* = 5 to 6 biological replicates) or subcutaneously injected with (B) LLC lung cancer cells (*N* = 7 to 9 biological replicates) and (C) B16F10 melanoma cancer cells (*N* = 5 biological replicates). Two-way analysis of variance (ANOVA) was used. (**D**) Immune and nonimmune cell composition of E0771, LLC, and B16F10 tumors and proportions of MPs as analyzed by flow cytometry (*N* = 4 biological replicates). (**E**) GO analysis of the genes that were uniquely up-regulated in E0771 *Prkcd*^{−/−} tumors. Bonferroni correction for multiple testing was used (**P* < 0.05, ***P* < 0.01, and *****P* < 0.0001). (**F**) Heatmap of median-centered mRNA expression of genes involved in the immune response in tumors from *Prkcd*^{+/+} and *Prkcd*^{−/−} mice (*N* = 5 to 6 biological replicates). (**G** to **I**) MHCII expression in macrophages and Ly6C^{hi} cells from (H) E0771 tumors and (I) spleens from same tumor bearing mice as quantified by mean fluorescence intensity (MFI; *N* = 4 to 5 biological replicates). (**J** and **K**) Flow cytometry analysis of CD3^{+}, CD4^{+}, and CD8^{+} T cell content in E0771 tumors reported as absolute cell numbers and frequency of live cells (*N* = 5 biological replicates). (**L**) Frequency of IFN-γ^{+} TNFα^{+} CD8^{+} T cells in E0771 tumors (*N* = 4 biological replicates). (**M**) CD8^{+} T cell and (**N**) PD-1^{+} CD8^{+} T cell content in LLC tumors (*N* = 6 to 9 biological replicates). Unpaired Student's *t* test was used in flow cytometry analysis (*P* < 0.05 was considered significant). Data are shown as means ± SEM. NK, natural killer.

Fig. 2. PKCδ is abundantly expressed by MPs in cancer. (**A** to **D**) *t*-distributed stochastic neighbor embedding (tSNE) plots of scRNA-seq showing major cell types, PRKCD mRNA expression, expression of monocyte/macrophage markers CD14 and CD68, T cell marker CD3E, and B cell marker CD19 in human (A) TNBC tumors using Wu *et al.*, dataset (*34*) and (C) melanoma tumors Jerby-Arnon *et al.* dataset (*35*). Percent of cells expressing the gene of interest and scaled mean expression is quantified with MPs highlighted in blue box [(B) and (D)]. (**E**) Representative tSNE dimensionality reduction plot showing concatenated flow cytometry analysis of live cell populations in E0771 tumors and PKCδ expression. MPs are highlighted (*N* = 4 biological replicates). (**F**) Representative histograms and (**G**) MFI quantification of PKCδ expression in the spleen and tumor MPs of E0771 tumor-bearing mice as quantified by MFI (*N* = 4 biological replicates). MFI for CD4, CD8, NK, and LysG⁺ cells is shown in (G). Paired *t* test was used (****P < 0.0001). (**H** and **I**) Wild-type BMDMs were polarized with mouse recombinant interleukin-4 (IL-4) (20 ng/ml) for 24 hours (red line) or left untreated as vehicle control (black line), with fluorescence minus one (FMO) control (gray). (H) Representative histogram and (I) MFI quantification of M1 marker CD86, M2 marker CD206, and PKCδ (*N* = 5 biological replicates). Unpaired Student's *t* test (P < 0.05 was considered significant). Data are shown as means ± SEM.

was also moderately up-regulated in T and NK cells, but not in Ly6G$^+$ cells (Fig. 2G). Thus, PKCδ expression correlated with more immunosuppressive MPs, which hints to a potential role in promoting immune suppression in MPs. Next, we checked PKCδ expression in M2-like (alternatively activated) polarized bone marrow–derived macrophages (BMDMs), which are known to be immunosuppressive and tumor promoting (19). M2-like BMDMs expressed lower levels of the M1 marker CD86 and higher levels of the M2 marker CD206, as expected. We also found that PKCδ expression was significantly higher in M2-like BMDMs compared to nonpolarized BMDMs (Fig. 2, H and I). Together, these findings suggest that PKCδ may be a critical controller of MP regulatory or immunosuppressive states.

PKCδ deficiency impairs tumor growth and immune suppression via MPs

To investigate whether PKCδ deficiency in MPs is required for tumor repression and T cell activation, we first depleted MPs in *Prkcd*$^{+/+}$ and *Prkcd*$^{-/-}$ E0771 tumor-bearing mice using a combination of anti-Ly6C monoclonal antibody and clodronate liposomes (40) (Fig. 3A). In accordance with previous reports (41–43), we observed that MP depletion significantly delayed tumor growth in wild-type mice (*Prkcd*$^{+/+}$) (Fig. 3, B and D). By contrast, MP depletion in *Prkcd*$^{-/-}$ mice did not delay tumor growth but instead promoted tumor growth to an extent that is comparable with *Prkcd*$^{+/+}$ mice (Fig. 3, C and D). These results indicate that PKCδ deficiency likely reprograms MPs from a protumor phenotype to an antitumor phenotype.

We next investigated whether PKCδ deficiency in M2-like BMDMs decreases their tumor-promoting and T cell–suppressive activity (Fig. 3E) (44, 45). Cancer cells (LLC) coinjected with *Prkcd*$^{-/-}$ M2-like BMDMs had a significant delay in tumor growth compared to LLC coinjected with *Prkcd*$^{+/+}$ M2-like BMDMs (Fig. 3F). We observed a significant increase in the activation (IFN-γ$^+$ TNFα$^+$) of CD8$^+$ (Fig. 3, G and H) and CD4$^+$ (Fig. 3, G to I) T cells from *Prkcd*$^{-/-}$ M2-like BMDMs + LLC tumors compared to *Prkcd*$^{+/+}$ M2-like BMDMs + LLC tumors. Coinjection of *Prkcd*$^{-/-}$ M2-like BMDMs with LLC cells resulted in a prolonged delay of tumor growth, which may be attributed to critical early interactions between BMDMs and other cells in the TME (46–48). Adoptively transferred BMDMs are likely diluted by host tumor-associated macrophages (TAMs) over time, which may have resulted in an early shift in the phenotype of tumor-infiltrating immune cells, which lead to delayed but not fully controlled tumor progression. By contrast, deletion of PKCδ in guide RNA–transduced OT-I CD8$^+$ T cells did not affect T cell proliferation in MC38–ovalbumin (OVA) tumors (fig. S4, A to E), suggesting that T cell–specific PKCδ does not affect intratumoral CD8$^+$ T cell proliferation and activation. Collectively, our findings suggest that PKCδ plays a critical role in controlling MP-induced effector T cell suppression and subsequent tumor promotion.

PKCδ deficiency enhances antigen-presenting and cross-presenting capacity of MPs

Antigen presentation to CD4$^+$ T cells and antigen cross-presentation to CD8$^+$ T cells are hallmark properties of antigen-presenting cells (APCs) to mount an effective antitumor immune response (49). We pulsed BMDMs and DCs isolated from *Prkcd*$^{+/+}$ and *Prkcd*$^{-/-}$ mice with OVA before incubation with H-2K^b–OVA

peptide-specific T cell receptor (TCR) transgenic OT-I CD8$^+$ T cells or OT-II CD4$^+$ T cells and measured T cell proliferation by analyzing the dilution of CellTrace Violet (CTV) proliferation dye. We found that *Prkcd*$^{-/-}$ BMDMs and DCs were superior at inducing OT-I CD8$^+$ (Fig. 3J) and OT-II CD4$^+$ (Fig. 3K) T cell proliferation compared to *Prkcd*$^{+/+}$ BMDMs and DCs. In addition, PKCδ deficiency in BMDMs and DCs significantly increased IFN-γ production in both OT-I and OT-II coculture supernatants as evaluated by enzyme-linked immunosorbent assay (ELISA) (Fig. 3L). Findings herein indicate that PKCδ is critical in regulating MP-mediated T cell activation.

Intrinsic loss of PKCδ triggers type I and type II IFN signaling in MPs

To understand how PKCδ regulates MPs, we performed transcriptome analysis using RNA-seq data from *Prkcd*$^{-/-}$ and *Prkcd*$^{+/+}$ M1-like BMDMs, stimulated DCs (DCstim), iMCs (fig. S5, A and B), and whole E0771 tumors. We identified 552, 754, and 219 genes that were up-regulated in *Prkcd*$^{-/-}$ M1 BMDMs, DCstim, and iMCs, respectively, whereas 391, 905, and 186 genes were down-regulated in these cells, respectively (Fig. 4, A, E, and I). GSEA revealed that hallmark pathways that are associated with a proinflammatory phenotype such as response to IFN-α/γ and inflammatory response were significantly enriched in M1 BMDMs and DCstim compared to unstimulated BMDM and DCs, respectively, suggesting that these cells have been successfully polarized toward a proinflammatory phenotype (fig. S5, C and D). GSEA revealed that response to IFN-α/γ hallmark pathways were consistently highly enriched in *Prkcd*$^{-/-}$ M1 BMDMs (Fig. 4, B to D), DCstim (Fig. 4, F to H), iMCs (Fig. 4, J to L), and E0771 tumors (Fig. 4, M to O), suggesting that type I and type II IFN signaling pathways are triggered in PKCδ-deficient MPs. We also observed elevated expression of genes involved in the response to type I IFN in *Prkcd*$^{-/-}$ E0771 tumors compared to *Prkcd*$^{+/+}$ tumors (fig. S6). By contrast, pathways significantly enriched in *Prkcd*$^{+/+}$ M1 BMDM, DCstim, iMCs, and E0771 tumors included hallmark gene sets involved in promotion of tumor growth and metastasis such as epithelial-to-mesenchymal transition (EMT) and angiogenesis as well as anti-inflammatory pathways such as bile acid metabolism and coagulation (50–52), which were consistently highly enriched in *Prkcd*$^{+/+}$ M1 BMDM, DCstim, iMCs, and E0771 tumors (fig. S7, A to E).

The gene sets induced by type I and type II IFNs overlap considerably, and both are essential to induce T cell activation and protective immunity (53). We therefore investigated commonly enriched genes between *Prkcd*$^{-/-}$ M1 BMDM, DCstim, iMCs, and E0771 tumors from both hallmark gene sets response to IFN-α (18 genes) (Fig. 4P) and response to IFN-γ (26 genes) (Fig. 4Q). We found 11 overlapping genes between the two IFN gene sets (Fig. 4R), which may represent the most commonly up-regulated IFN responsive genes in PKCδ-deficient MPs. Together, our findings reveal a potential role of PKCδ in promoting protumor and anti-inflammatory pathways while repressing type I and II IFN pathways in MPs.

PKCδ deficiency enhances anti–PD-1 therapy

The antitumor effect observed in *Prkcd*$^{-/-}$ mice prompted us to determine whether PKCδ deficiency can improve responsiveness to ICB. We chose the LLC tumor model previously reported as being relatively resistant to ICB (33, 54). LLC tumor-bearing
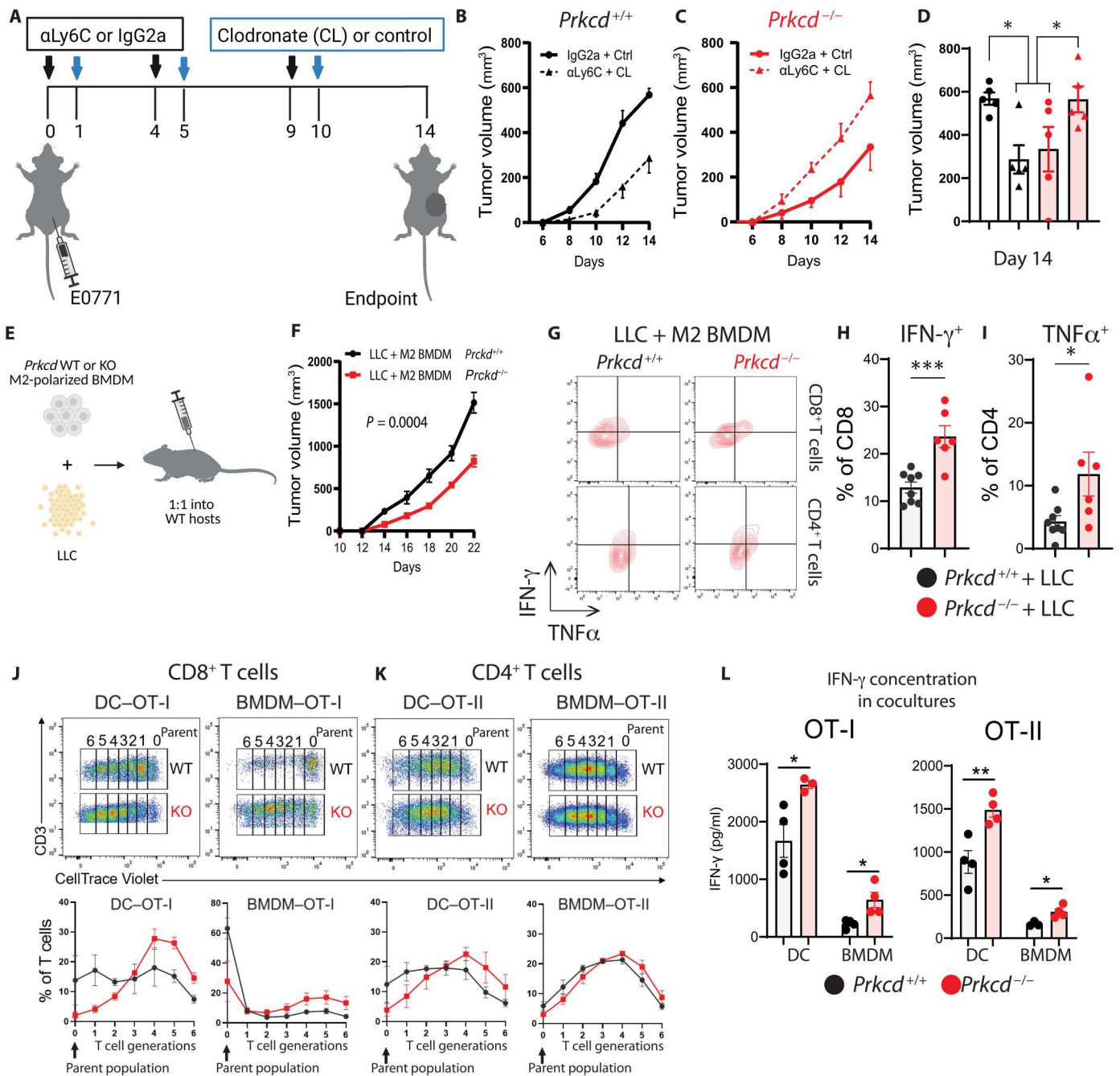
Fig. 3. Loss of PKCδ impairs tumor growth and immune suppression via MPs. *Prkcd*⁺/⁺ and *Prkcd*⁻/⁻ mice bearing E0771 tumors were treated with anti-Ly6C (αLy6C) or IgG2a monoclonal antibody (100 μg per mouse) followed by clodronate or control liposome (200 μl per mouse) as shown in experimental outline (**A**). Tumor volume in (**B**) *Prkcd*⁺/⁺ and (**C**) *Prkcd*⁻/⁻ mice and (**D**) tumor volumes at day 14 in *Prkcd*⁺/⁺ and *Prkcd*⁻/⁻ mice treated as in (A) are shown. One-way ANOVA with multiple comparisons with Tukey's correction was used (*$P < 0.05$). (**E** to **I**) LLC cells were coinjected with M2-polarized BMDMs (20 ng/ml of IL-4 for 24 hours) at a 1:1 ratio into wild-type mice. (E) Experimental outline and (F) tumor volume ($N = 8$ biological replicates). Two-way ANOVA was used. [(G) to (I)] Frequencies of IFN-γ⁺ TNFα⁺ (H) CD8⁺ and (I) CD4⁺ T cells in tumors from (E) and (F) was quantified and compared using unpaired Student's *t* test. (**J** to **L**) *Prkcd*⁺/⁺ or *Prkcd*⁻/⁻ bone marrow DCs and BMDMs were incubated with OVA (10 μg/ml) overnight before coculture with CTV-labeled CD8⁺ and CD4⁺ T cells isolated from OT-I and OT-II mice, respectively, for 3 days at a 2:1 T cell–DC/BMDM ratio. The individual peaks of CellTrace Violet dilution are highlighted as T cell generations ranging from 0 (parent population) to 6 (last daughter generation) and graphical representation of fractions of T cells in each peak in gated (J) CD8⁺ T cells and (K) CD4⁺ T cells. (L) IFN-γ concentration in OT-I and OT-II coculture supernatants from (J) and (K) was determined by ELISA ($N = 3$ to 4 biological replicates). Unpaired Student's *t* test (*$P < 0.05$, **$P < 0.01$, and ***$P < 0.001$). Data are shown as means ± SEM. WT, wild type; KO, knockout.
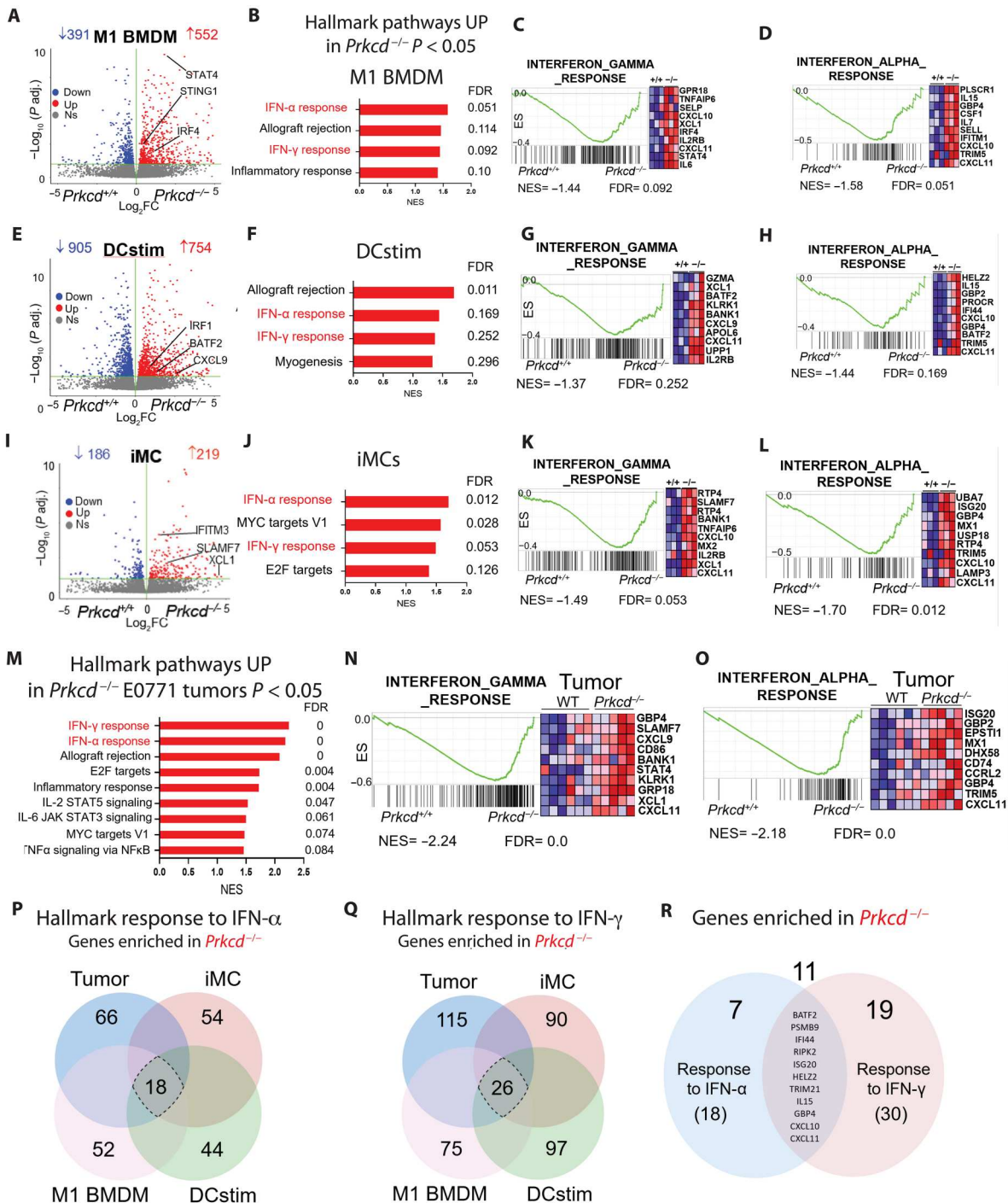
Fig. 4. Intrinsic loss of PKCδ triggers type I and type II IFN signaling in MPs. (**A**) Volcano plot for all DEGs between *Prkcd*$^{+/+}$ and *Prkcd*$^{-/-}$ M1 BMDMs is shown. Red = up; blue = down in *Prkcd*$^{-/-}$ relative to *Prkcd*$^{+/+}$. Number of genes up (red) or down (blue) in *Prkcd*$^{-/-}$ is noted above volcano plot relative to *Prkcd*$^{+/+}$. Ns, nonsignificant. (**B**) GSEA of the most significantly enriched gene sets in *Prkcd*$^{-/-}$ M1 BMDMs. (**C** and **D**) IFN-γ response and IFN-α GSEA plots for *Prkcd*$^{+/+}$ and *Prkcd*$^{-/-}$ M1 BMDMs. The top 10 enriched genes in *Prkcd*$^{-/-}$ relative to *Prkcd*$^{+/+}$ heatmap (red = up; blue = down from +1 to −1. (**E**) DEG between *Prkcd*$^{+/+}$ and *Prkcd*$^{-/-}$ DCstim. (**F**) GSEA of the most significantly enriched gene sets in *Prkcd*$^{-/-}$ DCstim. GSEA plot of the (**G**) IFN-γ response and (**H**) IFN-α response in *Prkcd*$^{+/+}$ and *Prkcd*$^{-/-}$ DCstim. (**I**) DEG between *Prkcd*$^{+/+}$ and *Prkcd*$^{-/-}$ iMCs. (**J**) GSEA of hallmark gene sets showing the most significantly enriched gene sets in *Prkcd*$^{-/-}$ iMCs. GSEA plot of the (**K**) IFN-γ response and (**L**) IFN-α response in *Prkcd*$^{+/+}$ and *Prkcd*$^{-/-}$ iMCs. (**M**) GSEA of hallmark gene sets showing the most significantly enriched gene sets in *Prkcd*$^{-/-}$ E0771 tumors compared to *Prkcd*$^{+/+}$. (**N** and **O**) IFN-γ and IFN-α GSEA response in *Prkcd*$^{+/+}$ and *Prkcd*$^{-/-}$ E0771 tumors. (**P** to **R**) Enriched genes in *Prkcd*$^{-/-}$ tumors, M1 BMDMs, DCstim, and iMCs for the hallmark gene sets (P) response to IFN-α and (Q) response to IFN-γ relative to *Prkcd*$^{+/+}$. (R) Venn diagrams of commonly enriched genes between *Prkcd*$^{-/-}$ tumors, M1 BMDMs, DCstim, and iMCs for response to IFN-α (18 common genes) and response to IFN-γ (26 common genes). *N* = 3 biological replicates for all MPs and *N* = 5 to 6 for E0771 tumors. NES, normalized enrichment score; FDR, false discovery rate; log2FC, log$_2$ fold change; JAK, Janus kinase; STAT, signal transducers and activators of transcription.

Prkcd^{+/+} and *Prkcd*^{−/−} mice were treated with anti–PD-1 or immunoglobulin G2a (IgG2a) control as outlined in Fig. 5A. Although we observed a moderate but significant reduction in tumor growth in *Prkcd*^{+/+} mice treated with anti–PD-1 compared to IgG2a-treated *Prkcd*^{+/+} mice, combination of PKCδ deficiency and anti–PD-1 synergistically delayed tumor growth (Fig. 5, B and C). Notably, *Prkcd*^{−/−} mice treated with anti–PD-1 had a significantly prolonged overall survival compared to other groups (Fig. 5D). Together, our findings indicate that PKCδ may represent a promising target to improve responsiveness to ICB.

DISCUSSION

Resistance to ICB poses a major challenge to the therapeutic management of patients with solid tumors. Now, most research efforts aiming at improving immunotherapy outcomes focus on T cells. However, given that innate immunity plays a critical role in orchestrating adaptive immunity, incorporating both arms of the immune system could be a more effective strategy to improve immunotherapy efficacy. In this study, we identified an immune evasion mechanism by which MPs are wired to suppress the antitumor immune response via PKCδ signaling. In this context, PKCδ acts as an innate immune checkpoint. We show that genetic deletion of PKCδ curbs tumor growth and promotes T cell tumor infiltration and activation in preclinical cancer models that have high MP content in their tumors. We also show that loss of PKCδ in MPs had a profound effect on the overall transcriptional program, which resulted in their reprogramming to an antitumor phenotype. PKCδ-deficient MPs activate type I and II IFN signaling, which are often required for mounting an antitumor immune response (55). These results highlight two key points: (i) the importance of MPs in controlling antitumor immunity and (ii) that PKCδ is a critical driver of MP phenotype in the TME and a potential target in cancer immunotherapy.

Although ICB has recently revolutionized cancer treatment, most patients fail to respond due to several factors, one of which is the establishment of a suppressive TME rich in myeloid cells (6). Thus, efforts are currently ongoing to identify additional myeloid targets to complement ICB. Some of these approaches focus on blocking suppressive MP cell recruitment to the TME, inhibiting their protumoral functions, or restoring their immunostimulatory properties. Among others, these approaches include inhibition of phosphoinositide 3-kinase gamma (56) and colony-stimulating factor 1 receptor (57), as well as blockade of triggering receptor expressed on myeloid cells 2 (TREM2) (6) and TAM receptors (Tyro3, Axl, and MerTK) (58). In our study, we found that PKCδ deficiency combined with anti–PD-1 markedly delayed tumor growth and significantly extended the survival of LLC tumor-bearing mice. Thus, PKCδ inhibition provides an exciting therapeutic approach that broadens the arsenal of myeloid cell targeting in tumors. Although several studies claim the existence of PKCδ specific inhibitors, one must be cautious using these inhibitors to specifically target the delta isoform of the PKC family due to several potential challenges (59). One of these challenges is off-target effects such as inhibition of other PKC isoforms that share similarities with the PKCδ protein structure. Some of these PKC isozymes may play contrasting physiological roles to PKCδ, which can result in dampening the desired effects of PKCδ inhibition (60). Therefore, developing therapeutic tools to specifically inhibit PKCδ

may represent a promising therapeutic strategy to enhance immunotherapy efficacy in patients with cancer.

PKCδ is a serine/threonine kinase of the novel PKC subfamily and can be activated by stimulation with diacylglycerol, leading to PKCδ phosphorylation and activation of downstream targets (25). PKCδ is involved in a myriad of cellular processes involving apoptosis, proliferation, and cell survival in a variety of cell types including immune cells (25, 26). In the hematopoietic compartment, studies have shown that genetic deletion of PKCδ resulted in systemic autoimmunity, which correlated with accumulation of autoreactive B cells in PKCδ knockout (KO) mice (27, 28). Similarly, patients with autosomal recessive PKCδ deficiency were severely autoimmune and suffered from systemic lupus erythematosus (26). In myeloid cells, previous work demonstrated that loss of PKCδ resulted in a defective reactive oxygen species production and impaired extracellular trap formation in neutrophils (29) and decreased macrophage phagosomal clearance of *Listeria monocytogenes* and *Mycobacterium tuberculosis* (30, 31). Moreover, we show that PKCδ is the most abundant PKC isoform in myeloid cells, with moderate T cell expression, which emphasizes an unappreciated role of this isoform in the regulation of myeloid cells. Although PKCδ is widely characterized as a pro-apoptotic protein in cancer cells, much of the literature is still conflicted as to whether PKCδ inhibits or promotes cancer cell growth (32). Our work aligns with previous studies by demonstrating that PKCδ plays a crucial role in regulating the immune response by acting as a brake on MP activation. Although this effect may be desirable at steady state to prevent autoimmunity (61), it is however detrimental in cancer where an immune response is necessary to control tumors. In our study, we show that PKCδ is consistently and abundantly expressed by MPs across several human tumors. We also found that PKCδ is variably expressed by B cells and cancer cells depending on the tumor or organ type. Previous studies show that PKCδ plays a role in the function of T cells and B cells in a noncancer setting (24). Our loss-of-function experimental results herein demonstrate that T cell–specific PKCδ loss does not affect tumor-specific CD8^{+} T cell proliferation in tumors. These data suggest that T cell PKCδ may not be critical to the TME, whereas PKCδ plays a greater role in regulating myeloid cell activation in the context of antitumor immunity. However, future studies are needed to decipher the role of PKCδ in other hematopoietic cells, such as T or B cells, and nonhematopoietic cells in cancer.

Our data also show that PKCδ expression correlates with an immunosuppressive TME. PKCδ is up-regulated in the TME (a more immunosuppressive microenvironment) compared to the spleen (a less immunosuppressive microenvironment). The specific mechanism of PKCδ up-regulation in the tumor compared to the spleen is unknown but is likely mediated by cell-cell interactions, metabolites, cyto/chemokines, or other factors yet to be discovered.

The underlying molecular mechanisms by which PKCδ dampens MP activation remain unclear. Our data suggest that this effect may be achieved by PKCδ activation of downstream pathways such as coagulation, bile acid metabolism, and EMT—all of which promote the protumor and/or anti-inflammatory phenotype in MPs. In our study, PKCδ was shown to repress type I and II IFN pathways through as yet unknown mechanisms, which are essential in orchestrating an effective T cell–mediated antitumor immune response (62). The exact molecular interactions by which PKCδ represses IFN signaling will be the subject of future investigations.
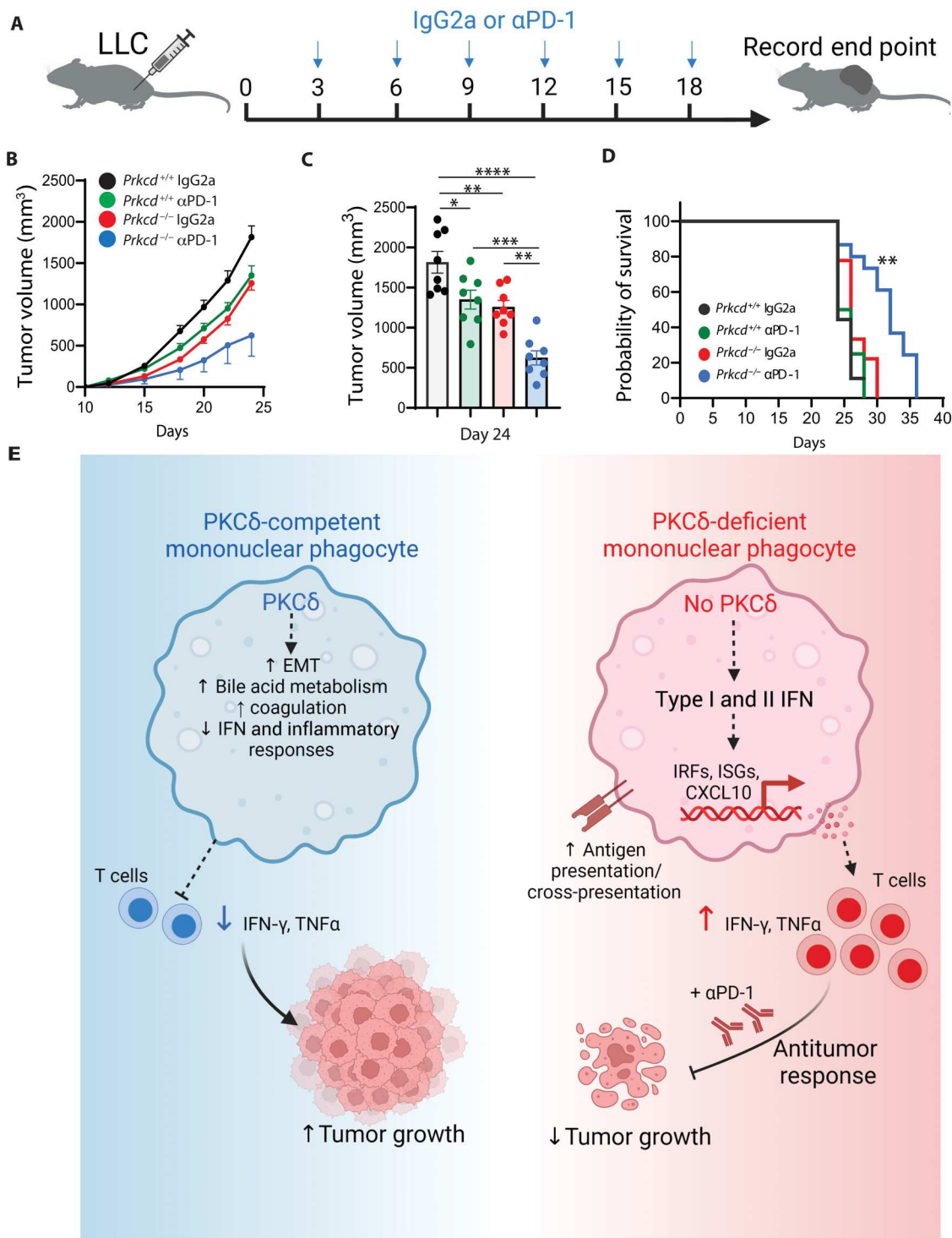
Fig. 5. Loss of PKCδ improves response to anti–PD-1 therapy. LLC tumor-bearing *Prkcd*^+/+^ and *Prkcd*^−/−^ mice were treated with anti–PD-1 (αPD-1) (200 μg per mouse) or IgG2a (200 μg per mouse) every 3 days as shown in (**A**). (**B**) Tumor volume over time until day 24, (**C**) tumor volume at day 24, and (**D**) Kaplan-Meier survival curves of tumor-bearing mice are shown (*N* = 8 mice per group). (**E**) Proposed model of PKCδ function in MPs and tumor progression. One-way ANOVA with multiple comparisons with Tukey's correction was used to compare tumor volumes (*$P < 0.05$, **$P < 0.01$, ***$P < 0.001$, and ***$P < 0.0001$). Data are shown as means ± SEM. Log-rank (Mantel-Cox) test was used to determine statistical significance for survival of mice in (E) (**$P < 0.01$, ***$P < 0.001$, and ***$P < 0.0001$). EMT, epithelial-to-mesenchymal transition.

While the evidence provided here is supportive toward targeting MP PKCδ, a limitation is that our models were syngeneic transplants. It remains to be seen whether targeting PKCδ will be a successful strategy against spontaneous tumorigenesis and more advanced disease. It will be important to design specific PKCδ inhibitors targeted to MPs because PKCδ also plays a role as a tumor suppressor in cancer cells (63, 64), which may limit the efficacy of these inhibitors. Another limitation is that constitutive PKCδ deficiency might trigger direct or indirect compensatory responses of MPs that affect tumor growth. It will be interesting to determine whether acute inhibition of PKCδ using specific pharmacological agents results in complete control of tumor progression. Future studies using specific PKCδ inhibitors will be important to demonstrate how pharmacological inhibition of PKCδ in MPs interferes with signaling pathways and how it affects tumor growth. A concern of targeting PKCδ is the potential for immune-related adverse events, as pathways such as IFN and antigen presentation are activated in the absence of PKCδ. Future work in the field would aim to limit adverse events. For example, cytotoxic T-lymphocytes associated protein 4 (CTLA-4) KO mice do not survive more than 3 weeks due to severe immune adverse events (65), yet anti−CTLA-4 therapy using monoclonal antibodies is well tolerated and FDA approved for the treatment of several cancer types. Additionally, effective targeted delivery of PKCδ inhibitors [for example, small interfering RNA (siRNA) or small molecule] to MPs is a viable approach to reprogram these cells in the TME as nanoparticle delivery to specific subsets of cells is advantageous and increasingly feasible. A large body of evidence shows that targeted delivery to MPs specifically can be achieved using nanoparticles such as liposomes or siRNA-loaded nanoparticles (66–68). Thus, approaches such as these will likely eliminate or reduce the impact of PKCδ inhibition in other cell types. In conclusion, this report demonstrates that PKCδ is a key driver of MP protumor phenotype in the TME, revealing a key target for cancer immunotherapy.

MATERIALS AND METHODS
Reagents
All reagents were obtained from Sigma-Aldrich (St. Louis, MO) unless otherwise noted. Fetal bovine serum (FBS; Gibco, Waltham, MA), 100× L-glutamine, 100× penicillin/streptomycin HyClone (Pittsburgh, PA), and Gibco 100× antibiotic mix were obtained from Thermo Fisher Scientific (Waltham, MA). RPMI 1640, Dulbecco's modified Eagle's medium (DMEM), and Matrigel are from Corning (Tewksbury, MA). Mouse recombinant granulocyte-macrophage colony-stimulating factor (GM-CSF), interleukin- 6 (IL-6), IL-4, macrophage CSF (M-CSF), and FMS-like tyrosine kinase 3 ligand (FLT3L) were obtained from BioLegend (San Diego, CA). OVA was obtained from Thermo Fisher Scientific. Mouse IFN-γ ELISA kit was obtained from R&D Systems (Minneapolis, MN). Mouse CD4+ T cell isolation kit and CD8+ T cell isolation kit were obtained from Miltenyi Biotec (Auburn, CA). Clodronate and control liposomes were obtained from Liposoma (Amsterdam, The Netherlands). In vivo anti-mouse CD40, anti-mouse PD-1, anti-mouse Ly6C monoclonal antibodies, and their controls (rat IgG2a) were all obtained from Bio X Cell (Lebanon, NH). KO-validated PKCδ antibody and phycoerythrin/Cy7 conjugation kit were obtained from Abcam (Cambridge, UK). Flow cytometry antibodies, compensation beads, and reagents are described in table S1 [Tonbo Biosciences Inc. (San Diego, CA), Thermo Fisher, and BioLegend].

Animals
Animal studies were performed with approval and in accordance with the guidelines of the Institutional Animal Care and Use Committee (IACUC) at the University of Tennessee Health Science Center (UTHSC) or Vanderbilt University Medical Center and in accordance with the National Institutes of Health Guide for the Care and Use of Laboratory Animals. All animals were housed in a temperature-controlled facility with a 12-hour light/12-hour dark cycle and ad libitium access to food and water. $Prkcd^{-/-}$ mice were a gift from Z. Dong at Augusta University, Augusta GA and were generated as previously described (69). After genotyping, only age- and sex-matched wild-type $Prkcd^{+/+}$ and $Prkcd^{-/-}$ mice were used in experiments. C57BL/6J (stock no. 000664) mice were purchased from the Jackson Laboratory (Bar Harbor, ME). For OT-I CD8+ T cell and OT-II CD4+ T cell studies, spleens from transgenic mice expressing the MHCI- restricted TCR specific for the octamer SIINFEKL peptide OVA 257 to 264 (OT-I mice) and MHCII-restricted TCR for the octamer SIINFEKL peptide OVA 323 to 339 (OT-II mice) were a gift from H. Chi at St Jude Children's Research Hospital, Memphis, TN. Recombination activating gene 1 (RAG1) KO mice (B6.129S7-$Rag1^{tm1Mom}$/J) were obtained from the Jackson Laboratory (strain # Jax 002216).

Tumor mouse models and OT-I T cell transduction
Eight- to 12-week-old sex-matched $Prkcd^{+/+}$ or $Prkcd^{-/-}$ mice were used in in vivo experiments. E0771-luciferase (luc), a gift from H. Korkaya, Augusta University, is a murine adenocarcinoma breast cancer cell line that was originally isolated from a C57BL/6 mouse spontaneous tumor. Cells were cultured and injected as we previously described (3). Briefly, cells were cultured in RPMI containing 10% FBS, penicillin (100 UI/ml), and streptomycin (100 µg/ml) in a humidified chamber at 37°C under 5% CO_2. E0771 cells were implanted into the left fourth mammary fat pad of 8-week-old C57BL/6J females at 250,000 cells in 100 µl of 25% Matrigel. Murine LLC cells (10^6 cells unless otherwise specified), a gift from J. A. Carson from the UTHSC, Memphis, TN, and murine B16F10 melanoma cells (3×10^5 cells), a gift from H. Chi at St. Jude Children's and Research Hospital in Memphis, TN were cultured in DMEM as above and were subcutaneously implanted in phosphate-buffered saline into the right flank of male mice as noted. For adoptive OT-I T cell transfer experiments, 1×10^6 MC38-OVA cells [gift from R. T. O'Neil (70)] were injected into the right flank of RAG1 KO mice (model, fig. S4A). Ten days later, splenocytes were isolated from OT-I;Cas9 double transgenic mice and activated in complete RPMI containing SIINFEKL peptide (1 µg/ml) and IL-2 (1 µg/ml). CD8+ T cells were isolated via negative magnetic bead selection following 48 hours of activation and transduced with either a green fluorescent protein (GFP)−expressing nontargeting control guide RNA as a control or blue fluorescent protein (BFP)−expressing PKCδ (Prkcd) targeting guide RNA via retroviral supernatant. Transduction efficiency was measured the following day by flow cytometry (fig. S4, B and C), and cells were mixed to achieve approximately 1:1 ratio of GFP: BFP−expressing cells. T cells (1×10^6) were then retro-orbitally injected into MC38-OVA tumor-bearing RAG1 KO mice. One week later, tumors were harvested, digested using Miltenyi tumor

digestion kit, and strained through a 70 μM nylon mesh filter. CD8+ T cells were isolated from the resulting single-cell suspension using Miltenyi-positive CD8+ T cell magnetic beads according to the manufacturer's protocol, stained, and analyzed by flow cytometry. The guide RNA sequences were as follows: nontargeting control: AAAACGGCTCGATCGGTGAT; *Prkcd*: 5′-CACCGAGCCCAC CATGTATCCTGAG-3′. Platinum-E Retroviral Packaging Cell Line was obtained from Cell Biolabs (RV-101, San Diego, CA). Tumor growth was monitored by measuring the length and width of the tumor using digital calipers. Tumor volume was calculated using the following formula (71): Volume = (width)^2 × (length)/2.

Anti–PD-1 tumor studies

Eight- to 12-week-old female $Prkcd^{+/+}$ or $Prkcd^{-/-}$ mice were implanted with LLC cells (2×10^5) as above. Mice from each genotype were randomized and then treated with six doses of anti–PD-1 or rat IgG2a (200 μg per mouse) every 3 days starting at day 3. Survival events were scored when tumor volume reached >2000 cm^3 or when mice had moribund appearance, reached end point per IACUC guidelines or per absolute survival.

In vivo MP depletion studies

MP depletion experiments were conducted as previously described (40) with some modifications. Briefly, 8- to 12-week-old $Prkcd^{+/+}$ or $Prkcd^{-/-}$ female mice were orthotopically implanted with E0771 cells (2.5×10^5) as above. Mice from each genotype were randomized then treated intraperitoneally with anti-Ly6C or rat IgG2a (100 μg per mouse) on day 0 followed by treatment with clodronate liposomes or control liposomes (200 μl per mouse) according to manufacturer's protocol on day 1. Anti-Ly6C or rat IgG2a treatments were given on days 0, 4, and 9, whereas clodronate or control liposomes were given on days 1, 5, and 10. Tumor volume was monitored until end point at day 14.

In vivo macrophage coinjection studies

Primary BMDMs from $Prkcd^{+/+}$ or $Prkcd^{-/-}$ female mice were polarized with IL-4 (20 ng/ml) to M2-like phenotype for 24 hours and collected into a single-cell suspension as previously described (44). Purified cells were mixed 1:1 with LLC cells, and 10^6 total cells were injected subcutaneously into the right flank of naive 8-week-old C57BL/6J female hosts. LLC cells alone (10^6) were used as a control. Tumor volume was measured every 2 days until end point.

Isolation of single cells from mouse tumors

Excised tumors (~300 mg) were minced using scissors in RPMI media containing enzyme cocktail mix from Miltenyi Biotec mouse tumor dissociation kit (Miltenyi Biotec, Auburn, CA). Tumor pieces were further digested as per the manufacturer's instructions, and digested tissue was filtered through 70-μm strainer to obtain a single-cell suspension. Spleen single-cell suspensions were obtained by grinding spleens against a 70-μm filter using a syringe plunger. Final single-cell suspensions were obtained following red blood cell lysis (MilliporeSigma, St. Louis, MO).

Flow cytometry analysis

Flow cytometry was performed as described in our previous study (16). Briefly, single-cell viability was determined by using Ghost dye (Tonbo Biosciences Inc.) followed by FcR blocking (Tonbo Biosciences Inc.). Antibodies were titrated, and the separation index was calculated using FlowJo v.10 software (Treestar, Woodburn, OR). Cells were stained with fluorescently labeled antibodies as previously described (16) and fixed with Foxp3/transcription factor staining buffer (Tonbo Biosciences Inc.). Stained cells were analyzed using Bio-Rad ZE5 flow cytometer in the UTHSC Flow Cytometry and Cell Sorting Core. A minimum number of 100 events were considered for analysis. Fluorescence minus one (FMO)–stained cells and single color UltraComp eBeads (Invitrogen, Carlsbad CA) were used as negative and positive controls, respectively.

For in vivo intracellular staining, tumor single-cell suspensions were stimulated with Cell Activation Cocktail (BioLegend) for 4 hours to allow the accumulation of intracellular cytokines according to the manufacturer's protocol. After staining with cell surface markers, single cells were fixed and permeabilized with Flow Cytometry Perm Buffer (Tonbo Biosciences Inc.) followed by staining with IFN-γ and TNFα.

Data were analyzed using FlowJo v.10 software. Flow cytometry *t*-distributed stochastic neighbor embedding plots were generated using the built-in plugin in FlowJo to project and cluster gated flow cytometry immune cell populations (16) (gating scheme shown in fig. S8). All antibodies and reagents are provided in table S1.

Isolation and stimulation of BMDMs, DCs, and iMCs

Bone marrow cells were isolated from the femurs and tibias of $Prkcd^{+/+}$ or $Prkcd^{-/-}$ age-matched females and were cultured in complete RPMI media (5×10^5 million cells/ml) supplemented with 50 μM β-mercaptoethanol, 10 mM Hepes, and 1 mM MEM nonessential amino acids (all Thermo Fisher Scientific). BMDMs were obtained after 6 days of culture with M-CSF (50 ng/ml). BMDMs were left unstimulated or further polarized to an M1-like phenotype (M1 BMDMs) with IFN-γ (20 ng/ml) and lipopolysaccharide (LPS) (100 ng/ml) or to an M2-like phenotype (M2 BMDMs) with IL-4 (20 ng/ml) for 24 hours (72). Bone marrow DCs were obtained after 7 days of culture with FLT3L (100 ng/ml) and then left unstimulated or stimulated (DCstim) with LPS (100 ng/ml) and anti-mouse agonistic CD40 monoclonal antibody (5 μg/ml) for 24 hours. Control DCs were treated with IgG2a (5 μg/ml). iMCs were obtained after bone marrow cells were cultured with GM-CSF (40 ng/ml) and IL-6 (40 ng/ml) for 6 days.

Antigen presentation and cross-presentation experiments and ELISA

CD4+ and CD8+ T cells were isolated from the spleens of tumor-free OT-II and OT-I mice, respectively, using magnetic-activated cell sorting (Miltenyi Biotec) according to the manufacturer's protocols and labeled with the proliferation dye CTV. Purity was >90% for all populations as verified by flow cytometry analysis. BMDMs and DCs were pulsed with OVA (10 μg/ml) for 24 hours before coculture with CD4+ (OT-II) and CD8+ (OT-I) T cells (105 cells) in a 96-well plate at a 1:2 APC–T cell ratio for 72 hours. Negative controls consisted of T cells cultured alone. T cell proliferation was assessed by CTV dilution within gated CD4+ and CD8+ T cells, respectively, and IFN-γ levels were assessed by ELISA (R&D Systems, Minneapolis, MN) in the coculture supernatants according to the manufacturer's protocol.

RNA sequencing

$Prkcd^{-/-}$ or $Prkcd^{+/+}$ freshly isolated mouse BMDMs, M1 BMDMs, DCs, DCstim and iMCs (n = 3 biological replicates each), as well as E0771 tumors (n = 5 to 6 biological replicates) were removed from dishes, and total RNA was collected using the RNeasy Mini Kit (QIAGEN) according to the manufacturer's instructions. The integrity of RNA was assessed using Agilent Bioanalyzer and samples with RNA integrity number > 5.0 were used. mRNA-seq libraries for the Illumina platform were generated and sequenced at GENEWIZ using the Illumina HiSeq 2 × 150–bp configuration following the manufacturer's protocol.

RNA-seq analysis

Fastq files from Illumina HiSeq that passed quality control processing using FastQC (73) were first aligned to the mouse transcriptome (mm10/GRCm38.p4 genome build with Ensembl v86 gene annotation) using STAR (74) and then sorted with SAMtools (75). Salmon (76) was then used for transcript quantification, and gene level counts were used for data analysis in R version 4.1.2 (77). Read counts were loaded from salmon quant files using tximport (78), and differential gene expression analysis between $Prkcd^{-/-}$ and $Prkcd^{+/+}$ groups was performed using DESeq2 (79). An adjusted P value < 0.1 was used to determine significantly DEGs from each sample group described in the previous section. Read counts were normalized for downstream analyses and visualization using the variance stabilizing transformation (VST) from DESeq2. Heatmaps representing VST normalized and scaled gene expression values were generated with the ComplexHeatmap package (80) where rows and/or columns were clustered via the "pearson" distance method. Significantly up-regulated genes in $Prkcd^{-/-}$ tumors, M1 BMDM, DCstim, and iMCs were used as the input for the GO Enrichment Analysis tool (81, 82). We performed a Bonferroni adjustment of gene set P values for the number of gene sets tested in the GO software using Fisher's exact test, and biological processes were ranked by fold enrichment. RNA-seq data are deposited in National Center for Biotechnology Information (NCBI) Gene Expression Omnibus (GEO) GSE208394.

Gene set enrichment analysis

For identification of enriched gene signatures, we used GSEA software (83). GSEA analysis was performed by using VST-normalized gene expression data obtained from E0771 tumors, M1 BMDM, DCstim, and iMCs (N = 5 to 6 for tumor and N = 3 biological replicates for other cell types). We used 1000 gene set permutations to test for significance at a false discovery rate threshold of 0.25. The MSigDB hallmark gene sets (H collection) (84) were used to determine enriched pathways in $Prkcd^{-/-}$ and $Prkcd^{+/+}$ groups. The top 10 ranked enriched genes by enrichment score in $Prkcd^{-/-}$ groups are shown in a heatmap next to the corresponding GSEA enrichment plot (Fig. 4 and fig. S7). Normalized enrichment score are reported. For GSEA hallmark gene sets, nominal P value was less than 0.05 for all shown pathways. For volcano plots, DEGs with an adjusted P value less than 0.1 were considered.

scRNA-seq analysis

$PRKCD$ expression was analyzed in different immune cell populations within healthy or tumor human and mouse tissues using the online tool "Single Cell Portal" from the Broad Institute (https://singlecell.broadinstitute.org/single_cell). We used the following publicly available scRNA-seq datasets: human TNBC tumors [Wu et al. (34)], human melanoma tumors [Jerby-Arnon et al. (35)], human renal cell carcinoma tumors [Bi et al. (36)], human colon cancer tumors [Pelka et al. (37)], human glioblastoma tumors [Neftel et al. (38)], human PBMCs (Broad/Boston and Mt. Sinai/NYC), and mouse $CD45^+$ splenocytes (ImmGen labs).

Statistical methods

Sample size for tumor studies were based on the effects observed in pilot studies, and power calculations were based on tumor growth studies. Power calculations were performed to ensure that the null hypothesis would be correctly rejected with >80% power at 0.05 significance. For in vivo depletion and anti–PD-1 studies, mice were randomly assigned to experimental groups. Statistical differences between experimental groups were determined by unpaired Student's t tests for comparisons between two groups and one-way or two-way analysis of variance (ANOVA) with Tukey's correction for multiple comparisons or two-way ANOVA with repeated measures to model longitudinal tumor growth between groups. Log-rank (Mantel-Cox) test was used to determine statistical significance for survival of mice. Statistical analysis was performed using the software within GraphPad Prism (GraphPad Software Inc., La Jolla, CA). All data are shown as means ± SEM. P values less than 0.05 were considered statistically significant.

Supplementary Materials

This PDF file includes:
Figs. S1 to S8
Legend for table S1

Other Supplementary Material for this manuscript includes the following:
Table S1

REFERENCES AND NOTES

1. M. Chaib, S. C. Chauhan, L. Makowski, Friend or Foe? Recent strategies to target Myeloid cells in cancer. *Front. Cell Dev. Biol.* **8**, 351 (2020).

2. D. Bruni, H. K. Angell, J. Galon, The immune contexture and Immunoscore in cancer prognosis and therapeutic efficacy. *Nat. Rev. Cancer* **20**, 662–680 (2020).

3. A. K. Pingili, M. Chaib, L. M. Sipe, E. J. Miller, B. Teng, R. Sharma, J. R. Yarbro, S. Asemota, Q. al Abdallah, T. S. Mims, T. N. Marion, D. Daria, R. Sekhri, A. M. Hamilton, M. A. Troester, H. Jo, H. Y. Choi, D. N. Hayes, K. L. Cook, R. Narayanan, J. F. Pierre, L. Makowski, Immune checkpoint blockade reprograms systemic immune landscape and tumor microenvironment in obesity-associated breast cancer. *Cell Rep.* **35**, 109285 (2021).

4. A. Ribas, J. D. Wolchok, Cancer immunotherapy using checkpoint blockade. *Science* **359**, 1350–1355 (2018).

5. G. Morad, B. A. Helmink, P. Sharma, J. A. Wargo, Hallmarks of response, resistance, and toxicity to immune checkpoint blockade. *Cell* **184**, 5309–5337 (2021).

6. M. Molgora, E. Esaulova, W. Vermi, J. Hou, Y. Chen, J. Luo, S. Brioschi, M. Bugatti, A. S. Omodei, B. Ricci, C. Fronick, S. K. Panda, Y. Takeuchi, M. M. Gubin, R. Faccio, M. Cella, S. Gilfillan, E. R. Unanue, M. N. Artyomov, R. D. Schreiber, M. Colonna, TREM2 modulation remodels the tumor myeloid landscape enhancing anti-PD-1 immunotherapy. *Cell* **182**, 886–900.e17 (2020).

7. M. Chaib, U. A. Tanveer, L. Makowski, Myeloid cells in the era of cancer immunotherapy: Top 3 unanswered questions. *Pharmacol. Ther.* **244**, 108370 (2023).

8. D. Laoui, E. van Overmeire, K. Movahedi, J. van den Bossche, E. Schouppe, C. Mommer, A. Nikolaou, Y. Morias, P. de Baetselier, J. A. van Ginderachter, Mononuclear phagocyte heterogeneity in cancer: Different subsets and activation states reaching out at the tumor site. *Immunobiology* **216**, 1192–1202 (2011).

9. Z. Duan, Y. Luo, Targeting macrophages in cancer immunotherapy. *Signal Transduct. Target. Ther.* **6**, 127 (2021).

10. M. F. Gutknecht, A. H. Bouton, Functional significance of mononuclear phagocyte populations generated through adult hematopoiesis. *J. Leukoc. Biol.* **96**, 969–980 (2014).

11. K. C. Lam, R. E. Araya, A. Huang, Q. Chen, M. di Modica, R. R. Rodrigues, A. Lopès, S. B. Johnson, B. Schwarz, E. Bohrnsen, A. P. Cogdill, C. M. Bosio, J. A. Wargo, M. P. Lee, R. S. Goldszmid, Microbiota triggers STING-type I IFN-dependent monocyte reprogramming of the tumor microenvironment. *Cell* **184**, 5338–5356.e21 (2021).

12. A. Chow, B. D. Brown, M. Merad, Studying the mononuclear phagocyte system in the molecular age. *Nat. Rev. Immunol.* **11**, 788–798 (2011).

13. T. S. Griffith, S. R. Wiley, M. Z. Kubin, L. M. Sedger, C. R. Maliszewski, N. A. Fanger, Monocyte-mediated tumoricidal activity via the tumor necrosis factor-related Cytokine, TRAIL. *J Exp Med* **189**, 1343–1354 (1999).

14. R. N. Hanna, C. Cekic, D. Sag, R. Tacke, G. D. Thomas, H. Nowyhed, E. Herrley, N. Rasquinha, S. McArdle, R. Wu, E. Peluso, D. Metzger, H. Ichinose, I. Shaked, G. Chodaczek, S. K. Biswas, C. C. Hedrick, Patrolling monocytes control tumor metastasis to the lung. *Science* **350**, 985–990 (2015).

15. B. Z. Qian, J. Li, H. Zhang, T. Kitamura, J. Zhang, L. R. Campion, E. A. Kaiser, L. A. Snyder, J. W. Pollard, CCL2 recruits inflammatory monocytes to facilitate breast-tumour metastasis. *Nature* **475**, 222–225 (2011).

16. M. Chaib, L. M. Sipe, J. R. Yarbro, M. S. Bohm, B. R. Counts, U. Tanveer, A. K. Pingili, D. Daria, T. N. Marion, J. A. Carson, P. G. Thomas, L. Makowski, PKC agonism restricts innate immune suppression, promotes antigen cross-presentation and synergizes with agonistic CD40 antibody therapy to activate CD8+ T cells in breast cancer. *Cancer Lett.* **531**, 98–108 (2022).

17. F. Veglia, M. Perego, D. Gabrilovich, Myeloid-derived suppressor cells coming of age. *Nat. Immunol.* **19**, 108–119 (2018).

18. T. Kwak, F. Wang, H. Deng, T. Condamine, V. Kumar, M. Perego, A. Kossenkov, L. J. Montaner, X. Xu, W. Xu, C. Zheng, L. M. Schuchter, R. K. Amaravadi, T. C. Mitchell, G. C. Karakousis, C. Mulligan, B. Nam, G. Masters, N. Hockstein, J. Bennett, Y. Nefedova, D. I. Gabrilovich, Distinct populations of immune-suppressive macrophages differentiate from monocytic myeloid-derived suppressor cells in cancer. *Cell Rep.* **33**, 108571 (2020).

19. A. Mantovani, F. Marchesi, A. Malesci, L. Laghi, P. Allavena, Tumour-associated macrophages as treatment targets in oncology. *Nat. Rev. Clin. Oncol.* **14**, 399–416 (2017).

20. M. Binnewies, A. M. Mujal, J. L. Pollack, A. J. Combes, E. A. Hardison, K. C. Barry, J. Tsui, M. K. Ruhland, K. Kersten, M. A. Abushawish, M. Spasic, J. P. Giurintano, V. Chan, A. I. Daud, P. Ha, C. J. Ye, E. W. Roberts, M. F. Krummel, Unleashing Type-2 dendritic cells to drive protective antitumor CD4(+) T cell immunity. *Cell* **177**, 556–571.e16 (2019).

21. M. L. Broz, M. Binnewies, B. Boldajipour, A. E. Nelson, J. L. Pollack, D. J. Erle, A. Barczak, M. D. Rosenblum, A. Daud, D. L. Barber, S. Amigorena, L. J. van't Veer, A. I. Sperling, D. M. Wolf, M. F. Krummel, Dissecting the tumor myeloid compartment reveals rare activating antigen-presenting cells critical for T cell immunity. *Cancer Cell* **26**, 638–652 (2014).

22. H. Salmon, J. Idoyaga, A. Rahman, M. Leboeuf, R. Remark, S. Jordan, M. Casanova-Acebes, M. Khudoynazarova, J. Agudo, N. Tung, S. Chakarov, C. Rivera, B. Hogstad, M. Bosenberg, D. Hashimoto, S. Gnjatic, N. Bhardwaj, A. K. Palucka, B. D. Brown, J. Brody, F. Ginhoux, M. Merad, Expansion and activation of CD103(+) dendritic cell progenitors at the tumor site enhances tumor responses to therapeutic PD-L1 and BRAF inhibition. *Immunity* **44**, 924–938 (2016).

23. S. Hegde, V. E. Krisnawan, B. H. Herzog, C. Zuo, M. A. Breden, B. L. Knolhoff, G. D. Hogg, J. P. Tang, J. M. Baer, C. Mpoy, K. B. Lee, K. A. Alexander, B. E. Rogers, K. M. Murphy, W. G. Hawkins, R. C. Fields, C. J. DeSelm, J. K. Schwarz, D. G. DeNardo, Dendritic cell paucity leads to dysfunctional immune surveillance in pancreatic cancer. *Cancer Cell* **37**, 289–307.e9 (2020).

24. B. Maier, A. M. Leader, S. T. Chen, N. Tung, C. Chang, J. LeBerichel, A. Chudnovskiy, S. Maskey, L. Walker, J. P. Finnigan, M. E. Kirkling, B. Reizis, S. Ghosh, N. R. D'Amore, N. Bhardwaj, C. V. Rothlin, A. Wolf, R. Flores, T. Marron, A. H. Rahman, E. Kenigsberg, B. D. Brown, M. Merad, A conserved dendritic-cell regulatory program limits antitumour immunity. *Nature* **580**, 257–262 (2020).

25. E. Salzer, E. Santos-Valente, S. Keller, K. Warnatz, K. Boztug, Protein kinase C δ: A gatekeeper of immune homeostasis. *J. Clin. Immunol.* **36**, 631–640 (2016).

26. A. L. Neehus, K. Moriya, A. Nieto-Patlán, T. le Voyer, R. Lévy, A. Özen, E. Karakoc-Aydiner, S. Baris, A. Yildiran, E. Altundag, M. Roynard, K. Haake, M. Migaud, K. Dorgham, G. Gorochov, L. Abel, N. Lachmann, F. Dogu, S. Haskologlu, E. İnce, J. el-Benna, G. Uzel, A. Kiykim, K. Boztug, M. R. Roderick, M. Shahrooei, P. A. Brogan, H. Abolhassani, G. Hancioglu, N. Parvaneh, A. Belot, A. Ikinciogullari, J. L. Casanova, A. Puel, J. Bustamante, Impaired respiratory burst contributes to infections in PKCδ-deficient patients. *J. Exp. Med.* **218**, e20210501 (2021).

27. A. Miyamoto, K. Nakayama, H. Imaki, S. Hirose, Y. Jiang, M. Abe, T. Tsukiyama, H. Nagahama, S. Ohno, S. Hatakeyama, K. I. Nakayama, Increased proliferation of B cells and auto-immunity in mice lacking protein kinase Cδ. *Nature* **416**, 865–869 (2002).

28. A. Limnander, P. Depeille, T. S. Freedman, J. Liou, M. Leitges, T. Kurosaki, J. P. Roose, A. Weiss, STIM1, PKC-δ and RasGRP set a threshold for proapoptotic Erk signaling during B cell development. *Nat. Immunol.* **12**, 425–433 (2011).

29. F. Soroush, Y. Tang, K. Guglielmo, A. Engelmann, E. Liverani, A. Patel, J. Langston, S. Sun, S. Kunapuli, M. F. Kiani, L. E. Kilpatrick, Protein kinase C-delta (PKCδ) tyrosine phosphorylation is a critical regulator of neutrophil-endothelial cell interaction in inflammation. *Shock* **51**, 538–547 (2019).

30. A. Schwegmann, R. Guler, A. J. Cutler, B. Arendse, W. G. C. Horsnell, A. Flemming, A. H. Kottmann, G. Ryan, W. Hide, M. Leitges, C. Seoighe, F. Brombacher, Protein kinase C delta is essential for optimal macrophage-mediated phagosomal containment of Listeria monocytogenes. *Proc. Natl. Acad. Sci. U.S.A.* **104**, 16251–16256 (2007).

31. S. P. Parihar, M. Ozturk, M. J. Marakalala, D. T. Loots, R. Hurdayal, D. B. Maasdorp, M. van Reenen, D. E. Zak, F. Darboe, A. Penn-Nicholson, W. A. Hanekom, M. Leitges, T. J. Scriba, R. Guler, F. Brombacher, Protein kinase C-delta (PKCδ), a marker of inflammation and tuberculosis disease progression in humans, is important for optimal macrophage killing effector functions and survival in mice. *Mucosal Immunol.* **11**, 496–511 (2018).

32. R. Garg, L. G. Benedetti, M. B. Abera, H. Wang, M. Abba, M. G. Kazanietz, Protein kinase C and cancer: What we know and what we do not. *Oncogene* **33**, 5225–5237 (2014).

33. S. I. Mosely, J. E. Prime, R. C. A. Sainson, J.-O. Koopmann, D. Y. Q. Wang, D. M. Greenawalt, M. J. Ahdesmaki, R. Leyland, S. Mullins, L. Pacelli, D. Marcus, J. Anderton, A. Watkins, J. C. Ulrichsen, P. Brohawn, B. W. Higgs, M. McCourt, H. Jones, J. A. Harper, M. Morrow, V. Valge-Archer, R. Stewart, S. J. Dovedi, R. W. Wilkinson, Rational selection of syngeneic preclinical tumor models for immunotherapeutic drug discovery. *Cancer Immunol. Res.* **5**, 29–41 (2017).

34. S. Z. Wu, D. L. Roden, C. Wang, H. Holliday, K. Harvey, A. S. Cazet, K. J. Murphy, B. Pereira, G. al-Eryani, N. Bartonicek, R. Hou, J. R. Torpy, S. Junankar, C. L. Chan, C. E. Lam, M. N. Hui, L. Gluch, J. Beith, A. Parker, E. Robbins, D. Segara, C. Mak, C. Cooper, S. Warrier, A. Forrest, J. Powell, S. O'Toole, T. R. Cox, P. Timpson, E. Lim, X. S. Liu, A. Swarbrick, Stromal cell diversity associated with immune evasion in human triple-negative breast cancer. *EMBO J.* **39**, e104063 (2020).

35. L. Jerby-Arnon, P. Shah, M. S. Cuoco, C. Rodman, M. J. Su, J. C. Melms, R. Leeson, A. Kanodia, S. Mei, J. R. Lin, S. Wang, B. Rabasha, D. Liu, G. Zhang, C. Margolais, O. Ashenberg, P. A. Ott, E. I. Buchbinder, R. Haq, F. S. Hodi, G. M. Boland, R. J. Sullivan, D. T. Frederick, B. Miao, T. Moll, K. T. Flaherty, M. Herlyn, R. W. Jenkins, R. Thummalapalli, M. S. Kowalczyk, I. Cañadas, B. Schilling, A. N. R. Cartwright, A. M. Luoma, S. Malu, P. Hwu, C. Bernatchez, M. A. Forget, D. A. Barbie, A. K. Shalek, I. Tirosh, P. K. Sorger, K. Wucherpfennig, E. M. van Allen, D. Schadendorf, B. E. Johnson, A. Rotem, O. Rozenblatt-Rosen, L. A. Garraway, C. H. Yoon, B. Izar, A. Regev, A cancer cell program promotes T cell exclusion and resistance to checkpoint blockade. *Cell* **175**, 984–997.e24 (2018).

36. K. Bi, M. X. He, Z. Bakouny, A. Kanodia, S. Napolitano, J. Wu, G. Grimaldi, D. A. Braun, M. S. Cuoco, A. Mayorga, L. DelloStritto, G. Bouchard, J. Steinharter, A. K. Tewari, N. I. Vokes, E. Shannon, M. Sun, J. Park, S. L. Chang, B. A. McGregor, R. Haq, T. Denize, S. Signoretti, J. L. Guerriero, S. Vigneau, O. Rozenblatt-Rosen, A. Rotem, A. Regev, T. K. Choueiri, E. M. van Allen, Tumor and immune reprogramming during immunotherapy in advanced renal cell carcinoma. *Cancer Cell* **39**, 649–661.e5 (2021).

37. K. Pelka, M. Hofree, J. H. Chen, S. Sarkizova, J. D. Pirl, V. Jorgji, A. Bejnood, D. Dionne, W. H. Ge, K. H. Xu, S. X. Chao, D. R. Zollinger, D. J. Lieb, J. W. Reeves, C. A. Fuhrman, M. L. Hoang, T. Delorey, L. T. Nguyen, J. Waldman, M. Klapholz, I. Wakiro, O. Cohen, J. Albers, C. S. Smillie, M. S. Cuoco, J. Wu, M. J. Su, J. Yeung, B. Vijaykumar, A. M. Magnuson, N. Asinovski, T. Moll, M. N. Goder-Reiser, A. S. Applebaum, L. K. Brais, L. K. DelloStritto, S. L. Denning, S. T. Phillips, E. K. Hill, J. K. Meehan, D. T. Frederick, T. Sharova, A. Kanodia, E. Z. Todres, J. Jané-Valbuena, M. Biton, B. Izar, C. D. Lambden, T. E. Clancy, R. Bleday, N. Melnitchouk, J. Irani, H. Kunitake, D. L. Berger, A. Srivastava, J. L. Hornick, S. Ogino, A. Rotem, S. Vigneau, B. E. Johnson, R. B. Corcoran, A. H. Sharpe, V. K. Kuchroo, K. Ng, M. Giannakis, L. T. Nieman, G. M. Boland, A. J. Aguirre, A. C. Anderson, O. Rozenblatt-Rosen, A. Regev, N. Hacohen, Spatially organized multicellular immune hubs in human colorectal cancer. *Cell* **184**, 4734–4752.e20 (2021).

38. C. Neftel, J. Laffy, M. G. Filbin, T. Hara, M. E. Shore, G. J. Rahme, A. R. Richman, D. Silverbush, M. K. L. Shaw, C. M. Hebert, J. Dewitt, S. Gritsch, E. M. Perez, L. N. Gonzalez Castro, X. Lan, N. Druck, C. Rodman, D. Dionne, A. Kaplan, M. S. Bertalan, J. Small, K. Pelton, S. Becker, D. Bonal, Q. D. Nguyen, R. L. Servis, J. M. Fung, R. Mylvaganam, L. Mayr, J. Gojo, C. Haberler, R. Geyeregger, T. Czech, I. Slavc, B. V. Nahed, W. T. Curry, B. S. Carter, H. Wakimoto, P. K. Brastianos, T. T. Batchelor, A. Stemmer-Rachamimov, M. Martinez-Lage, M. P. Frosch, I. Stamenkovic, N. Riggi, E. Rheinbay, M. Monje, O. Rozenblatt-Rosen, D. P. Cahill, A. P. Patel, T. Hunter, I. M. Verma, K. L. Ligon, D. N. Louis, A. Regev, B. E. Bernstein, I. Tirosh, M. L. Suvà, An integrative model of cellular states, plasticity, and genetics for glioblastoma. *Cell* **178**, 835–849.e21 (2019).

39. K. Alicea-Torres, E. Sanseviero, J. Gui, J. Chen, F. Veglia, Q. Yu, L. Donthireddy, A. Kossenkov, C. Lin, S. Fu, C. Mulligan, B. Nam, G. Masters, F. Denstman, J. Bennett, N. Hockstein, A. Rynda-Apple, Y. Nefedova, S. Y. Fuchs, D. I. Gabrilovich, Immune suppressive activity of myeloid-derived suppressor cells in cancer requires inactivation of the type I interferon pathway. *Nat. Commun.* **12**, 1717 (2021).

40. A. M. Rowe, H. Yun, B. R. Treat, P. R. Kinchington, R. L. Hendricks, Subclinical Herpes Simplex Virus Type 1 Infections Provide Site-Specific Resistance to an Unrelated Pathogen. *J. Immunol.* **198**, 1706–1717 (2017).

41. S. M. Zeisberger, B. Odermatt, C. Marty, A. H. M. Zehnder-Fjällman, K. Ballmer-Hofer, R. A. Schwendener, Clodronate-liposome-mediated depletion of tumour-associated macrophages: A new and highly effective antiangiogenic therapy approach. *Br. J. Cancer* **95**, 272–281 (2006).

42. L. Zhang, K. Zhang, J. Zhang, J. Zhu, Q. Xi, H. Wang, Z. Zhang, Y. Cheng, G. Yang, H. Liu, X. Guo, D. Zhou, Z. Xue, Y. Li, Q. Zhang, Y. da, L. Liu, Z. Yin, Z. Yao, R. Zhang, Loss of fragile site-associated tumor suppressor promotes antitumor immunity via macrophage polarization. *Nat. Commun.* **12**, 4300 (2021).

43. T. Li, X. Li, A. Zamani, W. Wang, C. N. Lee, M. Li, G. Luo, E. Eiler, H. Sun, S. Ghosh, J. Jin, R. Murali, Q. Ruan, W. Shi, Y. H. Chen, c-Rel is a myeloid checkpoint for cancer immunotherapy. *Nat. Cancer* **1**, 507–517 (2020).

44. M. Liu, Z. Tong, C. Ding, F. Luo, S. Wu, C. Wu, S. Albeituni, L. He, X. Hu, D. Tieri, E. C. Rouchka, M. Hamada, S. Takahashi, A. A. Gibb, G. Kloecker, H. G. Zhang, M. Bousamra II, B. G. Hill, X. Zhang, J. Yan, Transcription factor c-Maf is a checkpoint that programs macrophages in lung cancer. *J. Clin. Invest.* **130**, 2081–2096 (2020).

45. H. Yin, X. Zhang, P. Yang, X. Zhang, Y. Peng, D. Li, Y. Yu, Y. Wu, Y. Wang, J. Zhang, X. Ding, X. Wang, A. Yang, R. Zhang, RNA m6A methylation orchestrates cancer growth and metastasis via macrophage reprogramming. *Nat. Commun.* **12**, 1394 (2021).

46. D. I. Gabrilovich, S. Ostrand-Rosenberg, V. Bronte, Coordinated regulation of myeloid cells by tumours. *Nat. Rev. Immunol.* **12**, 253–268 (2012).

47. Z. Lu, J. Zou, S. Li, M. J. Topper, Y. Tao, H. Zhang, X. Jiao, W. Xie, X. Kong, M. Vaz, H. Li, Y. Cai, L. Xia, P. Huang, K. Rodgers, B. Lee, J. B. Riemer, C. P. Day, R. W. C. Yen, Y. Cui, Y. Wang, Y. Wang, W. Zhang, H. Easwaran, A. Hulbert, K. B. Kim, R. A. Juergens, S. C. Yang, R. J. Battafarano, E. L. Bush, S. R. Broderick, S. M. Cattaneo, J. R. Brahmer, C. M. Rudin, J. Wrangle, Y. Mei, Y. J. Kim, B. Zhang, K. K. H. Wang, P. M. Forde, J. B. Margolick, B. D. Nelkin, C. A. Zahnow, D. M. Pardoll, F. Housseau, S. B. Baylin, L. Shen, M. V. Brock, Epigenetic therapy inhibits metastases by disrupting premetastatic niches. *Nature* **579**, 284–290 (2020).

48. M. Casanova-Acebes, E. Dalla, A. M. Leader, J. LeBerichel, J. Nikolic, B. M. Morales, C. Chang, L. Troncoso, S. T. Chen, A. Sastre-Perona, M. D. Park, A. Tabachnikova, M. Dhainaut, P. Hamon, B. Maier, C. M. Sawai, E. Agulló-Pascual, M. Schober, B. D. Brown, B. Reizis, T. Marron, E. Kenigsberg, C. Moussion, P. Benaroch, J. A. Aguirre-Ghiso, M. Merad, Tissue-resident macrophages provide a pro-tumorigenic niche to early NSCLC cells. *Nature* **595**, 578–584 (2021).

49. M. Y. Lee, J. W. Jeon, C. Sievers, C. T. Allen, Antigen processing and presentation in cancer immunotherapy. *J. Immunother. Cancer* **8**, e001111 (2020).

50. C. Guo, S. Xie, Z. Chi, J. Zhang, Y. Liu, L. Zhang, M. Zheng, X. Zhang, D. Xia, Y. Ke, L. Lu, D. Wang, Bile acids control inflammation and metabolic disorder through inhibition of NLRP3 inflammasome. *Immunity* **45**, 802–816 (2016).

51. L. M. Sipe, M. Chaib, A. K. Pingili, J. F. Pierre, L. Makowski, Microbiome, bile acids, and obesity: How microbially modified metabolites shape anti-tumor immunity. *Immunol. Rev.* **295**, 220–239 (2020).

52. C. Wu, W. Lu, Y. Zhang, G. Zhang, X. Shi, Y. Hisada, S. P. Grover, X. Zhang, L. Li, B. Xiang, J. Shi, X. A. Li, A. Daugherty, S. S. Smyth, D. Kirchhofer, T. Shiroishi, F. Shao, N. Mackman, Y. Wei, Z. Li, Inflammasome activation triggers blood clotting and host death through pyroptosis. *Immunity* **50**, 1401–1411.e4 (2019).

53. S. Kumar, Z. Zeng, A. Bagati, R. E. Tay, L. A. Sanz, S. R. Hartono, Y. Ito, F. Abderazzaq, E. Hatchi, P. Jiang, A. N. R. Cartwright, O. Olawoyin, N. D. Mathewson, J. W. Pyrdol, M. Z. Li, J. G. Doench, M. A. Booker, M. Y. Tolstorukov, S. J. Elledge, F. Chédin, X. S. Liu, K. W. Wucherpfennig, CARM1 inhibition enables immunotherapy of resistant tumors by dual action on tumor cells and T cells. *Cancer Discov.* **11**, 2050–2071 (2021).

54. D. Ajona, S. Ortiz-Espinosa, T. Lozano, F. Exposito, A. Calvo, K. Valencia, M. Redrado, A. Remírez, F. Lecanda, D. Alignani, J. J. Lasarte, I. Macaya, Y. Senent, C. Bértolo, C. Sainz, I. Gil-Bazo, I. Eguren-Santamaría, J. M. Lopez-Picazo, A. Gonzalez, J. L. Perez-Gracia, C. E. de Andrea, S. Vicent, M. F. Sanmamed, L. M. Montuenga, R. Pio, Short-term starvation reduces IGF-1 levels to sensitize lung tumors to PD-1 immune checkpoint blockade. *Nat. Cancer* **1**, 75–85 (2020).

55. C. V. Rothlin, S. Ghosh, Lifting the innate immune barriers to antitumor immunity. *J. Immunother. Cancer* **8**, e000695 (2020).

56. M. M. Kaneda, K. S. Messer, N. Ralainirina, H. Li, C. J. Leem, S. Gorjestani, G. Woo, A. V. Nguyen, C. C. Figueiredo, P. Foubert, M. C. Schmid, M. Pink, D. G. Winkler, M. Rausch, V. J. Palombella, J. Kutok, K. McGovern, K. A. Frazer, X. Wu, M. Karin, R. Sasik, E. E. W. Cohen, J. A. Varner, PI3Kγ is a molecular switch that controls immune suppression. *Nature* **539**, 437–442 (2016).

57. D. A. Hume, K. P. MacDonald, Therapeutic applications of macrophage colony-stimulating factor-1 (CSF-1) and antagonists of CSF-1 receptor (CSF-1R) signaling. *Blood* **119**, 1810–1820 (2012).

58. Y. T. Akalu, C. V. Rothlin, S. Ghosh, TAM receptor tyrosine kinases as emerging targets of innate immune checkpoint blockade for cancer therapy. *Immunol. Rev.* **276**, 165–177 (2017).

59. S. P. Soltoff, Rottlerin: An inappropriate and ineffective inhibitor of PKCdelta. *Trends Pharmacol. Sci.* **28**, 453–458 (2007).

60. N. Qvit, D. Mochly-Rosen, The many hats of protein kinase Cδ: One enzyme with many functions. *Biochem. Soc. Trans.* **42**, 1529–1533 (2014).

61. M. Morell, N. Varela, C. Marañón, Myeloid populations in systemic autoimmune diseases. *Clin Rev Allergy Immunol* **53**, 198–218 (2017).

62. S. E. Fenton, D. Saleiro, L. C. Platanias, Type I and II interferons in the anti-tumor immune response. *Cancers (Basel)* **13**, 1037 (2021).

63. A. C. Newton, J. Brognard, Reversing the paradigm: Protein kinase C as a tumor suppressor. *Trends Pharmacol. Sci.* **38**, 438–447 (2017).

64. A. M. D'Costa, J. K. Robinson, T. Maudi, V. Chaturvedi, B. J. Nickoloff, M. F. Denning, The proapoptotic tumor suppressor protein kinase C-delta is lost in human squamous cell carcinomas. *Oncogene* **25**, 378–386 (2006).

65. S. C. Wei, W. C. Meijers, M. L. Axelrod, N. A. A. S. Anang, E. M. Screever, E. C. Wescott, D. B. Johnson, E. Whitley, L. Lehmann, P. Y. Courand, J. J. Mancuso, L. E. Himmel, B. Lebrun-Vignes, M. J. Wleklinski, B. C. Knollmann, J. Srinivasan, Y. Li, O. T. Atolagbe, X. Rao, Y. Zhao, J. Wang, L. I. R. Ehrlich, P. Sharma, J. E. Salem, J. M. Balko, J. J. Moslehi, J. P. Allison, A Genetic mouse model recapitulates immune checkpoint inhibitor-associated myocarditis and supports a mechanism-based therapeutic intervention. *Cancer Discov.* **11**, 614–625 (2021).

66. K. Uehara, T. Harumoto, A. Makino, Y. Koda, J. Iwano, Y. Suzuki, M. Tanigawa, H. Iwai, K. Asano, K. Kurihara, A. Hamaguchi, H. Kodaira, T. Atsumi, Y. Yamada, K. Tomizuka, Targeted delivery to macrophages and dendritic cells by chemically modified mannose ligand-conjugated siRNA. *Nucleic Acids Res.* **50**, 4840–4859 (2022).

67. X. Huang, C. Liu, N. Kong, Y. Xiao, A. Yurdagul Jr., I. Tabas, W. Tao, Synthesis of siRNA nanoparticles to silence plaque-destabilizing gene in atherosclerotic lesional macrophages. *Nat. Protoc.* **17**, 748–780 (2022).

68. S. S. Kim, C. Ye, P. Kumar, I. Chiu, S. Subramanya, H. Wu, P. Shankar, N. Manjunath, Targeted delivery of siRNA to macrophages for anti-inflammatory treatment. *Mol. Ther.* **18**, 993–1001 (2010).

69. W. H. Chou, D. S. Choi, H. Zhang, D. Mu, T. McMahon, V. N. Kharazia, C. A. Lowell, D. M. Ferriero, R. O. Messing, Neutrophil protein kinase Cdelta as a mediator of stroke-reperfusion injury. *J. Clin. Invest.* **114**, 49–56 (2004).

70. M. Z. Madden, X. Ye, C. Chi, E. L. Fisher, M. M. Wolf, G. A. Needle, J. E. Bader, A. R. Patterson, B. I. Reinfeld, M. D. Landis, E. S. Hathaway, J. E. Muka, R. T. O'Neil, J. Karijolich, M. Philip, J. C. Rathmell, Differential effects of glutamine inhibition strategies on antitumor CD8 T cells. *J. Immunol.* **211**, 563–575 (2023).

71. A. Faustino-Rocha, P. A. Oliveira, J. Pinho-Oliveira, C. Teixeira-Guedes, R. Soares-Maia, R. G. da Costa, B. Colaço, M. J. Pires, J. Colaço, R. Ferreira, M. Ginja, Estimation of rat mammary tumor volume using caliper and ultrasonography measurements. *Lab Anim (NY)* **42**, 217–224 (2013).

72. A. J. Freemerman, L. Zhao, A. K. Pingili, B. Teng, A. J. Cozzo, A. M. Fuller, A. R. Johnson, J. J. Milner, M. F. Lim, J. A. Galanko, M. A. Beck, J. E. Bear, J. D. Rotty, L. Bezavada, H. S. Smallwood, M. A. Puchowicz, J. Liu, J. W. Locasale, D. P. Lee, B. J. Bennett, E. D. Abel, J. C. Rathmell, L. Makowski, Myeloid Slc2a1-deficient murine model revealed macrophage activation and metabolic phenotype are fueled by GLUT1. *J. Immunol.* **202**, 1265–1286 (2019).

73. S. Andrews, A quality control tool for high throughput sequence data (2010); http://www.bioinformatics.babraham.ac.uk/projects/fastqc/.

74. A. Dobin, C. A. Davis, F. Schlesinger, J. Drenkow, C. Zaleski, S. Jha, P. Batut, M. Chaisson, T. R. Gingeras, STAR: Ultrafast universal RNA-seq aligner. *Bioinformatics* **29**, 15–21 (2013).

75. P. Danecek, J. K. Bonfield, J. Liddle, J. Marshall, V. Ohan, M. O. Pollard, A. Whitwham, T. Keane, S. A. McCarthy, R. M. Davies, H. Li, Twelve years of SAMtools and BCFtools. *Gigascience* **10**, giab008 (2021).

76. R. Patro, G. Duggal, M. I. Love, R. A. Irizarry, C. Kingsford, Salmon provides fast and bias-aware quantification of transcript expression. *Nat. Methods* **14**, 417–419 (2017).

77. R Core Team (*R Foundation for Statistical Computing*, 2021); https://www.R-project.org/.

78. C. Soneson, M. I. Love, M. D. Robinson, Differential analyses for RNA-seq: Transcript-level estimates improve gene-level inferences. *F1000Res* **4**, 1521 (2015).

79. M. I. Love, W. Huber, S. Anders, Moderated estimation of fold change and dispersion for RNA-seq data with DESeq2. *Genome Biol.* **15**, 550 (2014).

80. Z. Gu, R. Eils, M. Schlesner, Complex heatmaps reveal patterns and correlations in multi-dimensional genomic data. *Bioinformatics* **32**, 2847–2849 (2016).

81. H. Mi, A. Muruganujan, D. Ebert, X. Huang, P. D. Thomas, PANTHER version 14: More genomes, a new PANTHER GO-slim and improvements in enrichment analysis tools. *Nucleic Acids Res.* **47**, D419–d426 (2019).

82. Gene Ontology Consortium, The Gene Ontology resource: Enriching a GOld mine. *Nucleic Acids Res.* **49**, D325–d334 (2021).

83. A. Subramanian, P. Tamayo, V. K. Mootha, S. Mukherjee, B. L. Ebert, M. A. Gillette, A. Paulovich, S. L. Pomeroy, T. R. Golub, E. S. Lander, J. P. Mesirov, Gene set enrichment analysis: A knowledge-based approach for interpreting genome-wide expression profiles. *Proc. Natl. Acad. Sci. U.S.A.* **102**, 15545–15550 (2005).

84. A. Liberzon, C. Birger, H. Thorvaldsdóttir, M. Ghandi, J. P. Mesirov, P. Tamayo, The Molecular Signatures Database (MSigDB) hallmark gene set collection. *Cell Syst* **1**, 417–425 (2015).